CRYOSYNTHESIS AND ENERGETICS OF SOME HIGHLY REACTIVE SMALL BORON COMPOUNDS AND GENERAL THEORETICAL REACTION KINETICS AT CRYOGENIC TEMPERATURES

A THESIS

Presented to

The Faculty of the Graduate Division

by

Partha Sarathi Ganguli

In Partial Fulfillment

of the Requirements for the Degree

Doctor of Philosophy in the School of Chemical Engineering

Georgia Institute of Technology

August, 1970

In presenting the dissertation as a partial fulfillment of the requirements for an advanced degree from the Georgia Institute of Technology, I agree that the Library of the Institute shall make it available for inspection and circulation in accordance with its regulations governing materials of this type. I agree that permission to copy from, or to publish from, this dissertation may be granted by the professor under whose direction it was written, or, in his absence, by the Dean of the Graduate Division when such copying or publication is solely for scholarly purposes and does not involve potential financial gain. It is understood that any copying from, or publication of, this dissertation which involves potential financial gain will not be allowed without written permission.

_____

7/25/68

CRYOSYNTHESIS AND ENERGETICS OF SOME HIGHLY REACTIVE SMALL BORON COMPOUNDS AND GENERAL THEORETICAL REACTION KINETICS AT CRYOGENIC TEMPERATURES

Approved:

Chairman

Date approved by Chairman: 8/28/70

ACKNOWLEDGMENTS

I am grateful to Dr. H. A. McGee, Jr., for his suggestion of cryosynthesis work and for his advice, interest, and encouragement during the progress of this research work. I wish to thank Dr. T. F. Moran and Dr. W. T. Ziegler for the interest and suggestions while serving on the reading committee. I am grateful to Professor M. J. S. Dewar for supplying us with some of his preprints and program listings.

I deeply appreciate the support of this research work by U. S. Air Force through grant AF-AFOSR-1308 and by the Georgia Tech Foundation. I also wish to thank Mrs. L. P. Gordon for her part in the theoretical molecular energetic calculations. The excellent typing by Mrs. Joyce Williams and Mrs. Betty Landers is also greatly appreciated.

The understanding and encouragement of my mother, brothers, sisters, and my other relatives are gratefully acknowledged.

TABLE OF CONTENTS

TABLE OF CONTENTS (Continued)

LIST OF TABLES

LIST OF ILLUSTRATIONS

SUMMARY

This thesis work, which is concerned with an experimental as well as a theoretical study of the cryogenic synthesis of some highly reactive or highly unstable compounds, has been reported in two parts. The first part, referred to as "Cryosynthesis and Molecular Energetics," involves the production of BH_3 and B_4H_8 by the pyrolysis of BH_3CO and B_4H_{10} respectively, the determination of the molecular energetics of BH_3CO by mass spectrometric techniques and of some B-H-F compounds using the new MINDO (Modified Intermediate Neglect of Differential Overlap) molecular orbital method. This part also involves the studies of the low-temperature stabilization of highly reactive borane and tetraborane(8) by a fast-flow pyrolysis and hard-quench technique in a cryogenic reactor-mass-spectrometer facility developed in this laboratory. The second part, referred to as "General Theoretical Reaction Kinetics," develops a general theoretical reaction formalism for kinetic computations using MO (Molecular Orbital) methods to study the useful existence of some highly reactive or unstable compounds at cryogenic temperatures.

Part I

Borane is an important molecule because of its high reactivity and its possible practical usefulness as a rocket propellant. Direct physical evidence for the BH_3 intermediate in the gas phase from mass spectrometric studies of diborane[1,4,5,6] and borane carbonyl[7,8,9] has

existed since 1964. The possibility that BH_3 might exist as a cryogenic material arose when a liquid helium quench of the products of a B_2H_6 microwave discharge produced an unidentified phase with a triple point of approximately 60°K[10]. There have been unsuccessful attempts to detect and stabilize borane by infra-red and mass spectrometric techniques by using pyrolysis or photolysis usually in combination with cryogenic matrix isolation[12,1,8].

Energetic studies on B_2H_6 and BH_3CO[4,6,7,11,13,17] reveal values of $D(BH_3\text{-}BH_3)$ determined mass spectrometrically to vary between 39 and 59 kcal/mole while values from kinetic experiments vary between 25 and 38 kcal/mole. The symmetric dissociation energy of diborane was clearly very controversial.

Tetraborane(8) B_4H_8, was observed[3,19,20] mass spectrometrically to be formed as a reaction intermediate in the pyrolysis of B_4H_{10}, B_4H_8CO, and B_5H_{11}. No earlier attempts have been made to isolate the species as a stable cryoreagent or to study its chemical reactivity and stability.

Pyrolysis studies of borane carbonyl were performed in a furnace inlet system with the exhaust port of the furnace virtually tangent to the ionizing electron beam of the ion source of the mass spectrometer. The pyrolysis temperature in a 4 mm i.d. x 4 cm long quartz furnace was around 250° at an input gas pressure of about 60 x 10^{-3} torr. Large concentrations of borane, BH_3, were produced. Significant decomposition of BH_3CO begins at about 220°, and with increasing temperature, the amount of BH_3CO decreases rapidly while that of both B_2H_6 and BH_3 increase. With increasing temperature above 250°, the amount of diborane increases while that of both BH_3CO and BH_3 decrease.

To study the cryogenic synthesis of borane from the pyrolysis of borane carbonyl, pyrolysis and rapid quenching experiments were performed with the furnace mounted inside a cryogenic quench and inlet arrangement attached to a mass spectrometer[12]. The monel walls of the quenching space were maintained at 65°-67°K. Refrigeration capacities limited experiments to about 40 min duration with furnace inlet pressures of BH_3CO of 1 to 100 x 10^{-3} torr and temperatures of 280° to 350°. Spectra during quenching at 67°K as well for some 16 min after the furnace and deposition had been turned off and with the composite frozen solid at 65°K showed the presence of free BH_3 and diborane. Authentic diborane is not detectable at this temperature. As the quenched solid then slowly warmed from 65°K, the spectra gradually became that of authentic diborane, and BH_3CO was observed above 90°K. It can be concluded that free BH_3 survives both transport through the quench-reactor and condensation and revaporization at 65°-67°K, and that the observed low temperature spectra are due to free BH_3 and B_2H_6 formed by recombination in the quench-reactor and in the ion source. The activation energy for recombination thus seems very low, and hence, the isolation of pure BH_3, as a useful cryogenic reagent unfortunately seems not very probable.

Pyrolysis experiments with B_4H_{10} were conducted in a furnace at 70° to 250° and with inlet pressures near 5 x 10^{-3} torr. B_4H_8 was observed as had been earlier reported[3].

Pyrolysis and quenching experiments with B_4H_{10} were conducted with the furnace mounted inside a U-tube quench-reactor at furnace temperatures of 220° to 250° and with B_4H_{10} inlet pressure near 5 x 10^{-3}

torr. The furnace effluent was quenched in the U-tube at 77°K. This trap-reactor was attached to a cryogenic inlet system of a mass spectrometer[23]. Subsequent warm-up and analysis of the quenched products show the spectra of both B_4H_8 and B_4H_{10} at temperatures from -135° to -100°. B_4H_8 must have survived the quench and revaporization, but the vapor pressures of B_4H_{10} and B_4H_8 are too similar to allow a separation of these B_4 species by simple distillation alone at very low temperatures. There was no evidence of decomposition of B_4H_8 or of its reaction either with itself or with B_4H_{10}. Higher boranes in the B_6, B_5, and B_7 region were observed at temperatures above -95°.

Ionization efficiency measurements at $m/_e$ 14 in the BH_3CO furnace effluent gas yielded $I(^{11}BH_3) = 12.24 \pm 0.1$ eV which is in good agreement with an earlier value from diborane pyrolysis[11]. The appearance potentials of $^{10}B^+$, $^{10}BH^+$, $^{10}BH_2^+$, and $^{11}BH_3^+$ from BH_3CO were also determined. These numbers, together with the corresponding data from the fragmentation and ionization of BH_3, permit a complete development of the molecular energetics of BH_3CO and a confirmation of $D(H_3B - BH_3) = 59$ kcal/mole. The value of $A(B^+)$ from BH_3CO appears to be inflated and will be discussed later.

The appearance potential data on BH_3CO and BH_3 permit three independent determinations of the bond dissociation energy, $D(BH_3 - CO)$, to be 1.46, 1.41, and 1.50 eV, respectively, and the resulting value of $D(BH_3 - CO) = 1.46$ eV or 33.7 kcal/mole seems well established. Convincing checks of the consistency of the data on BH_3CO, and those on B_2H_6 and BH_3 were developed. For example, from BH_3CO data, $D(BH_2^+ - H) = 0.66$ eV, while B_2H_6 AND BH_3 data yield $D(BH_2^+ - H) = 0.63$ and 0.62 eV,

respectively. Similarly, $D(BH^+ - H)$ = 0.80, 0.71, and 0.89 eV, respectively.

Using $D(BH_3 - CO)$ = 33.7 kcal/mole, the heat of atomization of BH_3 was calculated to be 257.5 kcal/mole; a similar calculation with data on B_2H_6[11] yields 256.5 kcal/mole. The calculation from B_2H_6 involved $D(BH_3 - BH_3)$ = 59 kcal/mole, and hence the indicated agreement suggests consistency as regards $D(BH_3 - BH_3)$ between the B_2H_6 and BH_3CO data. In addition, the observed equilibrium data[15] for the reaction, $2BH_3CO \rightleftharpoons B_2H_6 + 2CO$, gives the heat of reaction as, ΔH = 9.142 kcal/mole. Using this value and $D(BH_3 - CO)$ = 33.7 kcal/mole, one deduces $D(BH_3 - BH_3)$ = 58 kcal/mole which represents still another independent confirmation of the magnitude of $D(BH_3 - BH_3)$. This intermeshing consistency of data on both B_2H_6 and BH_3CO strongly suggests that the measurements on BH_3 do in fact refer to that species and not to a possible excited or partially opened diborane, $B_2H_6^*$.

The value of $A(B^+)$ from BH_3CO is 67 kcal/mole higher than it should be as indicated by the $\Delta H_{atom}(BH_3)$ calculation. A similar calculation showed $A(B^+)$ from B_2H_6 to be 1 eV too high, but the excess energy could reasonably be assigned to product H_2 appearing with 2 quanta of vibrational excitation. If we make this assignment also for the BH_3CO case, we must also assign 1.9 eV or 8 quanta of vibrational excitation to product CO to make the $A(B^+)$ value reasonable. The onset of significant cross sections for collisions producing products in closely spaced internal energy states will yield ionization efficiency data that can be easily misinterpreted. As has been similarly noted for hydrocarbons,[36] too low an ion concentration may also be the cause of the

high value of $A(B^+)$ due to the now greatly enhanced importance of instrumental sensitivity. The notion of one or more excited products is the simplest, although not definitive, explanation of the large value of $A(B^+)$.

An experimental search for the possible production of an excited BH_3^+ in the dissociative ionization of B_2H_6 has been made[37,38]. The absence of such excitation further supports the energetic arguments. If excitation had occurred in the appearance of BH_3^+ from B_2H_6, the observed AP would have exceeded the true value by the amount of this excitation, and the deduced value of $D(BH_3 - BH_3)$ would have been correspondingly too large.

To further understand these energetic arguments from a theoretical perspective, the new MINDO molecular orbital method[40] has been calibrated for B-H and B-F bonds. The MINDO method was selected because of its superior accuracy in calculations of heats of formation and ionization potentials for a wide variety of compounds. To calibrate the MINDO method for a certain kind of bond, one needs to determine the standard bond length and two empirical parameters, β^I and β^{II}, from fitting heat of formation data. Standard bond lengths in the MINDO method for small hydrocarbons were not significantly different from the actual ones, and so in our calculations experimental bond lengths were used. The MINDO calculated heat of atomization of BH_3 was 256 kcal/mole which is in excellent agreement with the measured value of 257 kcal/mole.

To inquire whether the parameters which correlate our experimental results on BH and BH_3 would also correctly predict the heat of formation of BHF_2, the B-F parameters were obtained by fitting an experimental

$\Delta H_f(BF_3)$ value. One then calculates $\Delta H_f(BHF_2) = -176.805$ kcal/mole which is in very good agreement with an experimental value of -175.7 ± 1.5 kcal/mole. This parametrization also permitted the computation of $\Delta H_f(BF) =$ 26.915 kcal/mole which is in good agreement with the experimental value of -29 ± 2.6 kcal/mole.

Computed and experimental ionization potential values are also in good agreements except for BF, but the experimental I(BF) value is questionable since it was measured at about 1300°. The difference between the calculated (11.92 eV) and the electron impact (12.24 ± 0.1 eV) ionization potential of BH_3 can be attributed to the difference between the adiabatic and vertical ionization potentials of the molecule.

The heat of atomization of BH_3 is 256.5 kcal/mole and 257.5 kcal/mole from completely independent sets of data measured in our laboratory on B_2H_6 ($D(BH_3 - BH_3) = 59$ kcal/mole) and BH_3CO ($D(BH_3CO) = 33.7$ kcal/mole) respectively. In both calculations only the values of $D(BH_3 - BH_3)$ and $D(BH_3 - CO)$ are significantly questionable. Reaction kinetic experiments have yielded $D(BH_3 - CO) = 23.1$ kcal/mole[7] and $D(BH_3 - BH_3) =$ 35 kcal/mole[17] both of which values yield a heat of atomization of BH_3 of about 269 kcal/mole. The parametrization of MINDO on this latter value yielded $\Delta H_f(BH) = 100.5$ kcal/mole which is outside of the experimental range.

All of these MINDO calculations suggest that there is a consistency in our energetic arguments that cannot be developed using other data. Also, the successful application of MINDO to B-H-F compounds demonstrates the broader applicability of this semi-empirical SCF-MO method.

Part II

A general approach has been proposed to determine the possibility of the cryogenic synthesis of unknown, but highly reactive, compounds. The useful existence of a compound becomes questionable when the compound is highly reactive or highly unstable. If the compound is highly reactive, it will react with itself to give less reactive products. In this case, one should study the bimolecular reaction characteristics of the compound at low temperature. An example of this behavior would be an exothermic dimerization reaction. If the compound is highly unstable, then one should study its exothermic unimolecular decomposition or isomerization reaction characteristics at low temperature. As a first step, these reactions at low temperatures but not at very low pressures have been studied theoretically in the gas phase for non-polar and non-ionic molecules.

Theoretical models have been proposed to study these chemical reactions at cryogenic temperatures. Assuming low activation energy and a relatively loose activated complex structure, a formulation of the specific rate constant for bimolecular gas phase reactions at cryogenic temperature has been developed using a statistical-dynamical model for the total chemical reaction cross-sections.

The computation method of the reaction characteristics of processes at cryogenic temperatures using the INDO[55] and MINDO/2[56] molecular orbital methods has been described briefly. The MINDO/2 method has been shown to give good estimates of bond lengths, heats of formation, and force constants simultaneously for a wide variety of hydrocarbons, thus satisfying the minimum requirements for a procedure to be used convincingly

for computing reaction characteristics. The INDO method has been shown to give good estimates of the equilibrium geometry, particularly, the bond angles of molecules. This method is, however, not good in calculations of molecular energetics. However, this method and also the MINDO/2 method can be justified as useful for the present purpose by the following arguments. Since the activated complex is loose, its identity is not much different from the reactants; so the errors involved in the calculation of their total energies will be in the same direction and almost of the same magnitude. Therefore when one calculates the activation energy by taking the difference of their total energies, those errors in the calculation should tend to cancel each other. Moreover, the errors inherent in the INDO approximations increase with decreasing distances as the neglected electron populations become more important. The minimum energy path for the reaction $CF_3 + CF_3 \rightarrow C_2F_6$ was computed by the INDO method. The computed activation energy for the reaction was < 1 kcal/mole. Assuming zero activation energy, the reaction was found experimentally to have a steric factor of 0.16[63]. This shows that the INDO method can be used in the present scheme of calculation. One can make these computations for molecules with atoms from the first row in the periodic table.

The minimum energy path, activated complex structure, and approximate activation energy for the reaction $BH_3 + BH_3 \rightarrow B_2H_6$ have been computed using the INDO molecular orbital method. The energies for different ways of approach and configurations were calculated. The minimum adiabatic energy path found for the process was as follows: (i) Approach of two borane molecules as shown below up to a B-B distance of 3.40 Å.

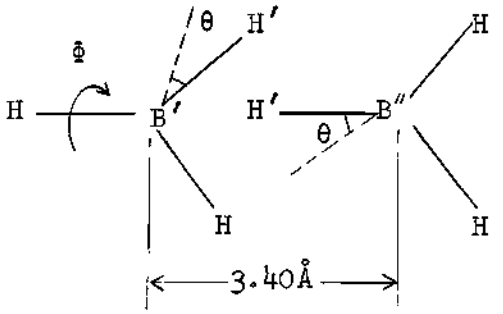

(ii) Then rotating $B'H_3$ in a clockwise direction with simultaneous twisting of B'H' and B"H' away from the plane in opposite directions as the two borane molecules approach each other. The activated complex structure is as shown below.

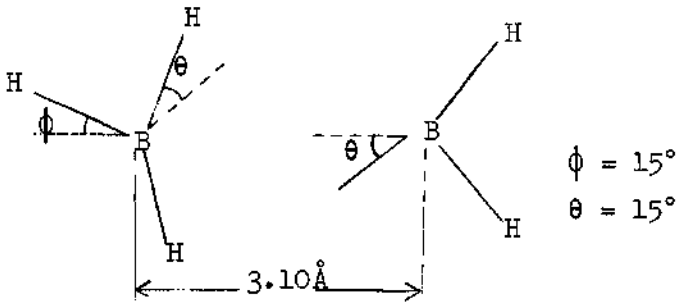

The activation energy obtained in this calculation is 1.849 kcal/mole, however, the accuracy of this value is questionable.

Considering the high reactivity of the borane molecule, the computed results look reasonable and support the postulate of a loose activated complex structure for gas phase reactions at cryogenic temperatures.

Experimental reaction kinetic studies of some reactions at cryogenic temperatures should be made to yield more insight into low temperature reactions. No such rate data on any system are now in existence. Reaction characteristics of such reactions at cryogenic temperatures,

particularly bimolecular reactions, should be computed in the way described in the present work and the chemical reactivity and stability features should be compared. Since the computation scheme depends upon the molecular orbital methods, one should use the best method available for the purpose assuming that there will continue to be further developments of these methods.

PART I

CRYOSYNTHESIS AND MOLECULAR ENERGETICS

CHAPTER I

INTRODUCTION

Definition and Brief History of the Problem

This thesis problem has been concerned with the cryogenic synthesis of some highly reactive and unstable compounds with practical and theoretical importance, and with the development of a general theoretical reaction kinetic method which will illuminate the useful existence of a compound at cryogenic temperatures. This includes the development of new or better synthesis techniques for these compounds, the determination of the molecular energetics of the systems studied (which facilitates the identification of the desired species as well as to calculate bond energies, heats of formation, etc.), and the stabilization of these compounds in a cryogenic reactor-mass-spectrometer facility. The theoretical reaction kinetics method includes the development of theoretical models for reactions at low temperature, the development of formulations of these models and the methods for their computation using recent molecular orbital methods.

Borane is one of the most important hydrides of the first row elements, because of its possible practical usefulness as a rocket propellant, and theoretically as an eight-electron system borane is also a molecule whose structure is of special interest to theoreticians for evaluating the accuracy of their ab initio computational techniques. The existence of borane is also important in the explanation of several

reaction mechanisms of boron hydride chemistry.

A brief history of the synthesis of borane in the gas phase was presented by Wilson[1] in which he made an unsuccessful attempt to stabilize borane at low temperature. Based on his electron impact data, Wilson also proposed a new value (59 kcal/mole) of the controversial symmetric dissociation energy of diborane which ranged from 27 to 55 kcal/mole without much certainty of any fixed value. Leroi[2] and Garnett[1e] made attempts to detect borane by infra-red techniques using pyrolysis and photolysis in combination with matrix isolation, but they were, for the most part, also unsuccessful.

The proposed reaction mechanisms of the pyrolysis of B_4H_{10} and several other boron hydrides postulate the existence of B_4H_8 as a reaction intermediate, and the species has been observed mass spectrometrically[3] in the pyrolysis of B_4H_{10}. Nothing was known about its reactivity, stability, structure, or the possibility of its existence as a pure cryochemical reagent.

Purpose of the Research

The main purpose of this thesis research has been to make an experimental as well as theoretical study of cryogenic synthesis of highly reactive or highly unstable compounds. Experimentally, the purpose is to synthesize BH_3 and B_4H_8 in the gas phase from the pyrolysis of BH_3CO and B_4H_{10} respectively, to determine the energetics of small boron compounds by electron impact measurements as well as by molecular orbital calculations, and to prepare BH_3 and B_4H_8 as a stable, isolable, condensed phase at cryogenic temperatures. Energetic determinations were

made to have more insight into the cryosynthesis of borane and also to establish exactly the controversial value of the symmetric dissociation energy of diborane.

Theoretically, a study was made to find a general reaction kinetic method for predicting the useful existence of a compound as a cryochemical reagent. This included the study of chemical reactivity, stability and thereby the possibility of cryogenic synthesis of a compound.

Literature Review

Borane

From 1950 through 1963 various kinds of indirect evidence for the existence of BH_3 molecule from different compounds and by different processes have been reported by various workers as has been well summarized by Wilson[1]. From 1964, there has been direct physical evidence for the BH_3 intermediate from mass spectrometric studies of diborane[1,4,5,6] and borane carbonyl[7,8,9].

Fehlner and Koski[7] studied the reaction $BH_3CO \rightarrow BH_3 + CO$ by pyrolysis in a low pressure flow system using a special mass spectrometer. The reaction was found to be first order in BH_3CO and homogeneous. The bond dissociation energy $D(H_3B\text{-}CO)$ was estimated from the data to be 23.1 ± 2 kcal/mole which gave $D(H_3B - BH_3) = 37.1 \pm 4$ kcal/mole. In this study BH_3 was also observed as confirmed by rough appearance potential measurements. Herstad, et al.,[9] investigated the pyrolysis of borane carbonyl using a mass spectrometer as the detector of a molecular beam issuing from a flow reactor. Their study gave a clear cut identification of BH_3 formed in the pyrolysis.

Bolz, Mauer, and Peiser[10] subjected diborane to a microwave discharge and quenched the products at liquid helium temperature. By means of X-ray diffraction a new phase was observed which exhibited a triple point of approximately 60°K. This unidentified phase was postulated to be BH_3, although the possibility that it was only a previously unreported metastable phase of B_2H_6 could not be ruled out.

Wilson and McGee[11] made mass spectrometric studies of the synthesis, energetics, and cryogenic stability of borane. BH_3 was synthesized by the pyrolysis of diborane. They made thorough appearance potential measurements of different ions and calculated the symmetric dissociation energy of diborane to be 2.56 eV or 59 kcal/mole. Using a cryogenically cooled mass spectrometric system they attempted to prepare BH_3 as a stable cryoreagent at temperatures down to 55°K but the results were negative. Leroi[2] attempted to detect borane by an infrared technique using pyrolysis and photolysis in combination with matrix isolation, but he was also unsuccessful. Garnett[18] in his thesis studied the pyrolysis products of diborane and borane carbonyl, and the photolysis products of borane carbonyl by an infra-red matrix isolation technique. He was unsuccessful in efforts to detect borane in his pyrolysis study. In the photolysis study he concludes, "Much remains to be done to explain fully the photolysis of borane carbonyl. We have assigned an absorption at 1134.2 cm^{-1} to ν_4 of BH_3." However, this detection of borane was not very convincing as acknowledged by the author himself.

Various kinetic studies on B_2H_6 and BH_3CO were made by different workers assuming BH_3 to be a reaction intermediate. In 1956, Bauer[13]

made an analysis of eight independent kinetic studies and was led to upper bounds for the symmetric dissociation energy of diborane which ranged from 27 to 38.4 kcal/mole. A thermochemical value of 28.4 kcal/mole[14] was comparable with these results. Bauer stated that the published mechanism for the decomposition of BH_3CO by Burg[15] was wrong and proposed an alternate mechanism. Later, Garabedian and Benson[16] showed that Burg's kinetic data on BH_3CO decomposition were in excellent agreement with his original mechanism and fixed the symmetric dissociation energy of diborane as lying between 32 and 38.3 kcal/mole. From the remaining seven kinetic studies considered by Bauer, they were led to the conclusion that in six systems no calculation of the value of the energy of dissociation of diborane was warranted, and the remaining one would have yielded a lower bound of 33 kcal/mole.

Burg and Fu[17] studied the decomposition of BH_3PF_3 by infrared procedures and suggested the same mechanism as found earlier for BH_3CO. Extrapolation of early stage rate data for BH_3PF_3 to zero time gave first order rate constants for the initial dissociation at three temperatures. These results, when combined with the overall equilibria, led to $D(BH_3 - BH_3) = 35.0$ kcal/mole. The assumptions involved in their studies were (a) Zero activation energy for the reverse of the initial dissociation, $BH_3CO \rightarrow BH_3 + CO$ and (b) complete neglect of the reverse reaction of the second step, $BH_3 + BH_3CO \rightarrow B_2H_6 + CO$.

Sinke, et al.,[6] studied the kinetics of B_2H_6 decomposition in a Knudsen-type cell in conjunction with a mass spectrometer, and from the observed equilibrium between BH_3 and B_2H_6 deduced a value of the dissociation energy of B_2H_6 of 55 kcal/mole. Fehlner and Koski[4] used a fast

flow pyrolysis technique and a mass spectrometer and measured by an electron impact method the $A(BH_3^+)$ from B_2H_6 to be equal to 13.1 ± 0.2 eV and $I(BH_3)$ = 11.4 ± 0.2 eV which yield 39 kcal/mole for the dissociation energy of B_2H_6.

So in summary, the previous workers failed to prepare borane as a stable cryoreagent, and the symmetric dissociation energy of diborane was quite controversial.

This literature review suggests need for (a) a better synthesis method of borane, (b) an attempt to prepare borane as a stable, isolable, condensed phase at cryogenic temperatures, and (c) more definite energetic studies to establish the exact value of the symmetric dissociation energy of diborane.

Tetraborane(8)

B_4H_8 was suggested as an intermediate in the pyrolysis of B_4H_{10} and B_2H_6 by several workers[19]. Baylis, et al.,[3] studied the intermediates produced in the pyrolysis of B_4H_{10} with an "integral furnace" mass spectrometer with reactor temperatures between 10° and 285° and a reactor pressure of B_4H_{10} ca. 4.8×10^{-3} torr. B_4H_8 was identified as an intermediate in the pyrolysis. Diborane as well as a combination of pentaboranes (B_5H_9 and B_5H_{11}), hexaborane, a combination of heptaboranes, octaborane, decaborane, and possibly nonaborane were also observed. Hollins and Stafford[20] studied the pyrolysis of $^{n}B_5H_9$, $^{10}B_4H_8CO$, and $^{10}B_5H_{11}$ at very low pressures in a mass spectrometer with an integral flow reactor. The pyrolysis study of B_5H_9 revealed no evidence for the formation of any reactive intermediates. In the pyrolysis of B_4H_8CO, B_4H_8 is the initial decomposition product; no monoborane or triborane

species were observed. Small amounts of pentaboranes and possibly diborane were observed, but no higher boranes. Appearance potentials were measured for all the major ions due to B_4H_8CO. A study of the pyrolysis of B_5H_{11} has shown B_4H_8 and BH_3 to be decomposition products. No triborane species could be observed; diborane and pentaborane(9) were observed, but no higher boranes could be detected under these experimental conditions. The appearance potential of $^{10}B_4H_8^+$ from $^{10}B_4H_8CO$ is 10.6 ± 0.5 eV and that from $^{10}B_4H_8$ produced in the pyrolysis of $^{10}B_4H_8CO$ at 225°, it is 10.19 ± 0.5 eV.

This literature review suggests an attempt to synthesize and isolate B_4H_8 as a stable cryochemical reagent to be followed by a study of its properties.

The structure of tetraborane(10)[19] is shown below. Applying the semitopological equations[66] (modified to treat vacant orbital structures), Dupont and Schaeffer[67] suggested two satisfactory structures for B_4H_8 as shown below:

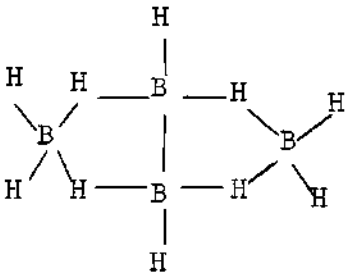

B_4H_{10}

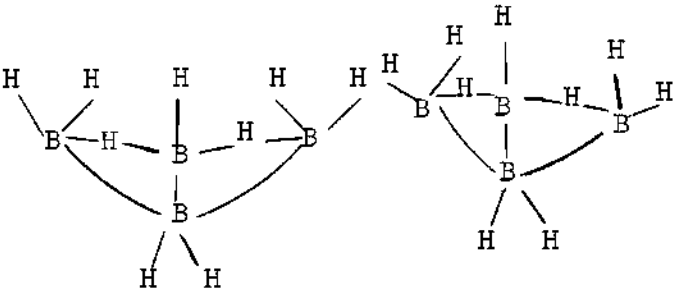

B_4H_8

CHAPTER II

APPARATUS AND EXPERIMENTAL PROCEDURES

Introduction

The major analytical device used in this thesis work was a Benxid Time-of-Flight Mass Spectrometer, Model 12-107. It permits one to identify a compound by mass spectral analysis and also to measure the appearance potentials of parent and fragment ions by electron impact methods. The description of this Mass Spectrometer, and its auxilliary facilities including the cryogenic arrangements that were developed in this laboratory were presented in several earlier theses[1,21,22].

Coaxial Furnace Inlet System

Two types of furnaces were used to conduct both pyrolysis and pyrolysis with immediate quenching experiments. For pyrolysis with immediate analysis of pyrolysis products, a tubular quartz or pyrex furnace was mounted coaxially with the drift tube of the mass spectrometer inside the fast reaction chamber (a) of the ion source header as shown in Figure 1. The exhaust port of the pyrolysis furnace can be positioned, by sliding through an O-ring sealed quick disconnect joint (b), at any point from being virtually tangent to the ionizing electron beam to about one inch away. The heated region (c) of the furnace tube, usually 4 cm in length, was wound with No. 28 gauge nichrome wire and

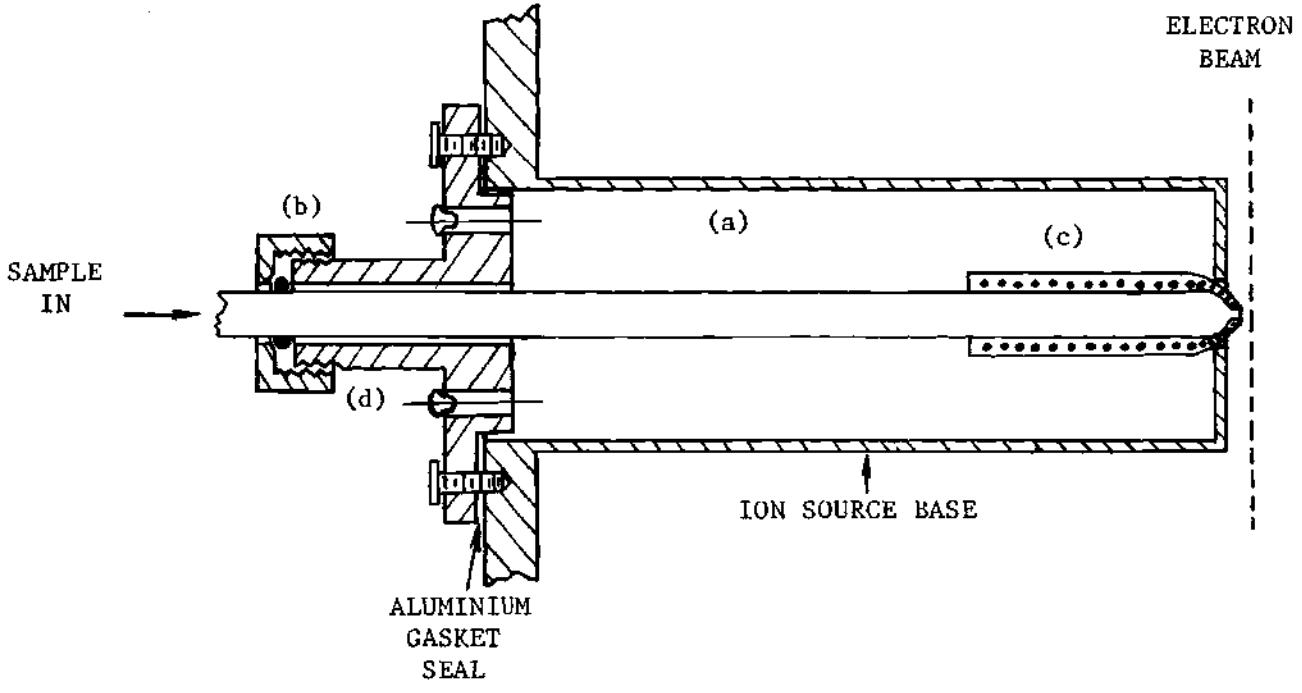

Figure 1. Coaxial Furnace Inlet System.

coated with Sauereisen Electrotemp cement for insulation as well as for uniform heating. Copper-constantan or chromel-alumel thermocouples were imbeded in the Sauereisen to measure the temperature of the furnace. High vacuum electrical feed throughs (d) soldered into a brass flange were used for the introduction of power and thermocouple leads.

The yield of the desired product in the pyrolysis depends upon temperature, pressure, furnace design, etc. In the BH_3CO pyrolysis experiments, the exhaust port of the furnace was virtually tangent to the ionizing electron beam of the ion source (the backing plate was removed from the ion source). Pyrolysis experiments were conducted in a 4 mm i.d. quartz furnace with its exhaust port constricted to 1 mm and with a 4 cm heated length. The pyrolysis temperature was about 250° at an input gas pressure of about 60×10^{-3} torr. The pressure is uncertain (indicated only by a thermocouple vacuum gauge), but it was readily maintained by thermostating the BH_3CO reactant reservoir at -153°, the freezing point of the convenient refrigerant, 2-methylpentane.

In the pyrolysis with immediate quenching experiments, another type of furnace as shown in Figure 2 was used. The heated portion, again about 4 cm long, was made at one end of the inner tube (5 mm o.d. pyrex) through which the reactant gas was passed. The inner tube with the furnace was then sealed inside a 10 mm o.d. pyrex tube. Therefore, the heated cement of the furnace and the gases evolved from these cement will not contaminate the pyrolysed and quenched products. The insulated power leads and the thermocouple wires emerged through an opening on the outer tube and were sealed by epoxy resin. Another opening on the outer tube was connected to a vacuum pump thereby keeping the annular space

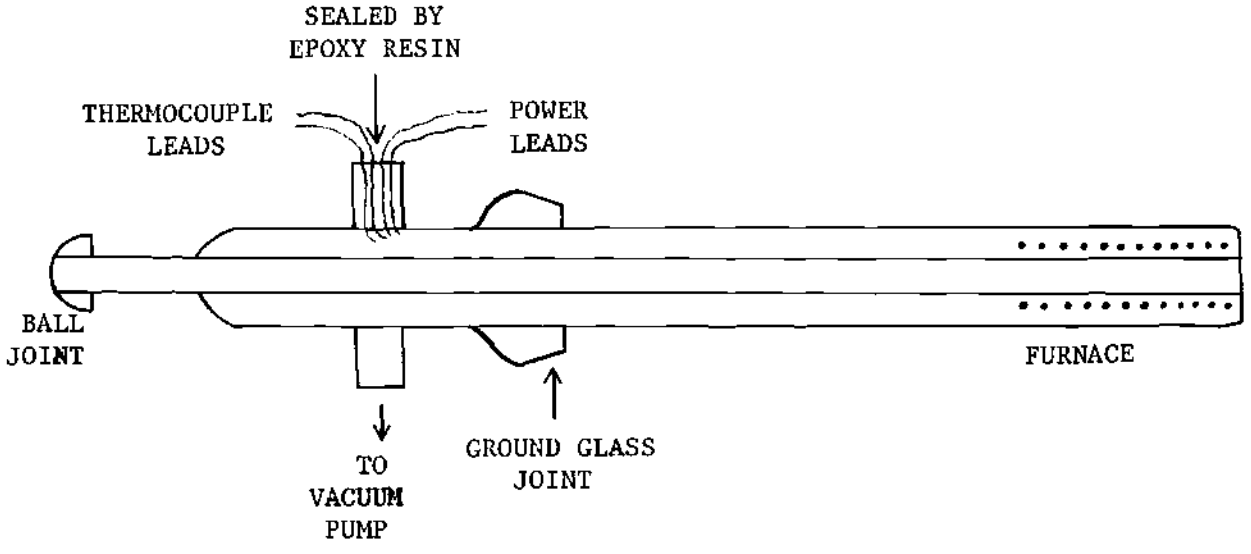

Figure 2. Sealed Furnace.

under vacuum for thermal insulation from the cryogenic trap. This ensures longer life of the heater wire and will also carry away water and other volatile gases which diffuse out of the heater cement. This vacuum will also lessen the heat transfer beyond the heated length. Due to the design features of the furnace described above, this type of furnace will be referred to as a "sealed furnace". One can cover the outer tube near the heated portion with aluminum-foil to reduce the radiation heating of the quenched products. A male ground glass joint is sealed on the outer tube for connection with a similar female joint on the cryogenic quench reactor assembly[12]. Using nicrhome heater on a pyrex tube, this furnace can be heated to 450°. However, it was possible to heat as high as 1200° by using platinum heater wire and the inner and outer tube near the heater made of quartz which was sealed to the remainder of the apparatus by a quartz to pyrex graded glass seal. The sealed furnace can also be fitted to the ion source header of the mass spectrometer simply by a brass flange with a quick disconnect joint for the purpose of pyrolysis and product analysis. No high vacuum electrical feed throughs are necessary in this case.

Cryogenic Inlet Systems

The cryogenic inlet system attached to the mass spectrometer is used for rapid quenching at low temperature of reactive or unstable compounds formed near to the quenching space by a suitable technique. By then warming the system in a controlled manner, it is possible to analyze mass-spectrometrically the different compounds as they evolve at different temperatures. The system is cooled by a suitable refrigerant, and it can

be simultaneously electrically heated and controlled by an automatic control system. Thus, the system can be automatically maintained at any temperature between that of the refrigerant and room temperature. The outlet port of the cryogenic inlet system can be positioned tangent to the ionizing electron beam so that the compounds are analyzed without warm-up. This inlet system can also be used for low temperature reactions and as a constant low temperature bath while making ionization potential measurements. The design considerations, mechanical descriptions and applications of the cryogenic inlet system A (Figure 3) used in the BH_3CO pyrolysis experiments have been described in detail in several thesis[1,21,22] from this laboratory and those of the cryogenic inlet system B used in the B_4H_{10} pyrolysis experiments have been described in detail by Holzhauer and McGee[23]. Only the auxiliary equipment and experimental procedures used in these pyrolysis and quench experiments will be described here.

A. Pyrolysis and Quench Experiments with BH_3CO

The pyrolysis and quench experiments with BH_3CO were carried out in a sealed furnace (Figure 2) with 4 mm i.d. x 4 cm long heated space and mounted within the cryogenic inlet system A.

The furnace was mounted inside and concentric with the 11 mm i.d. monel walls of the quenching space so that the furnace exit was just at the beginning of the quenching space. The distance from the furnace outlet port to the cold surface was then about 2.5 mm, and the quenching space was maintained below 10^{-6} torr by fast through-pumping. During pyrolysis and quench experiments the monel walls of the quenching space were maintained at 65°-67°K by using liquid oxygen refrigerant at low

pressure. The refrigerant chamber of the cryogenic inlet system was first flooded with liquid oxygen followed by pumping on the chamber with two high capacity mechanical pumps to produce the low starting temperature. The temperature was determined by measuring the pressure over the subcooled liquid oxygen as well as by a copper-constantan thermocouple. The temperature dropped from 90°K at first rapidly and then slowly to about 65°K. Once the low temperature was attained the furnace heater was turned on, which caused the temperature of the quenching space to rise to about 67°K. Refrigeration capacities limited pyrolysis experiments to about 40 minutes duration with furnace inlet pressures of BH_3CO of 1 to 100 x 10^{-3} torr and temperatures of 280° to 350°. It seemed that due to the effect of cold quenching space the apparent furnace temperature required for BH_3 production was more than without quenching. The furnace inlet pressures of BH_3CO were low enough to permit the pyrolysis to take place with the cryogenic inlet system extension piece advanced into place tangent to the electron beam. Hence the volatile species at the quenching temperature could be monitored during the product quench itself. After the pyrolysis was completed and the furnace had been turned off, the quenching space could be maintained at 65°K for about 16 minutes. After this time, the refrigerant chamber has lost all of its liquid oxygen, and no control over warm-up of the cryogenic inlet system was possible. However, as long as the refrigerant chamber was evacuated, the warm-up rate to room temperature was slow enough to permit reasonable mass spectrometric analyses of the evolved products at different temperatures.

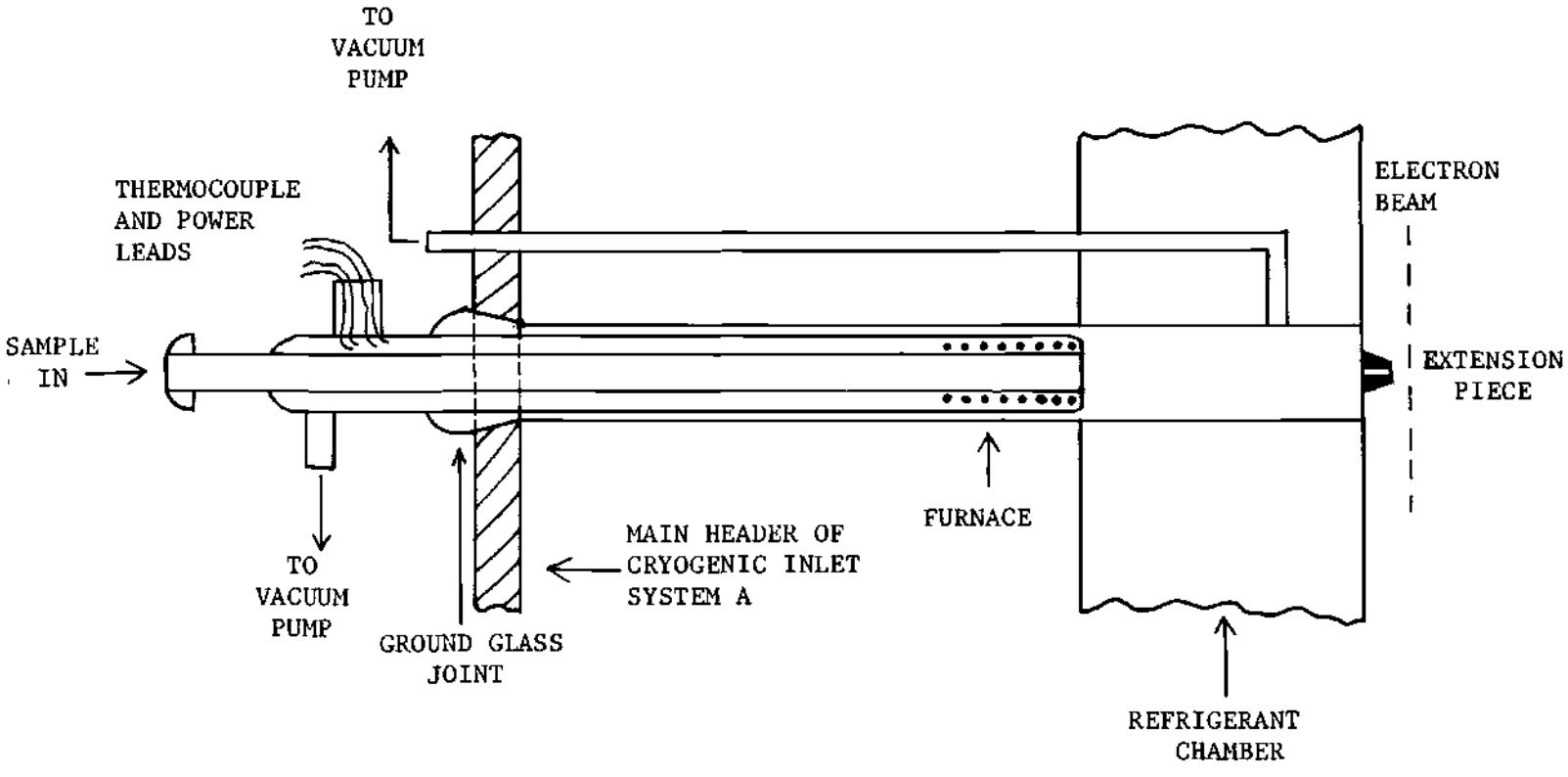

Figure 3. Sealed Furnace Inside Cryogenic Inlet System A.

B. Pyrolysis and Quenching Experiments with B_4H_{10}

The pyrolysis and quenching experiments of B_4H_{10} were conducted in a sealed furnace with 3 mm i.d. and 3.5 cm long heated space which was mounted on the cryogenic inlet system B in one side of a U-shaped pyrex tube (Figure 4). This tube was connected to the mass spectrometer and vacuum pump and was partly immersed in a suitable refrigerant. The distance from the furnace outlet port to the cold surface was about 4 mm, and the quenching space was maintained below 10^{-6} torr by fast through-pumping. During pyrolysis and quenching experiments the system was maintained at 77°K by immersion in liquid nitrogen. Pyrolysis and quenching experiments were conducted for about an hour with furnace inlet pressures of B_4H_{10} near 5×10^{-3} torr and temperatures of 220° to 250°. After the pyrolysis was completed and the furnace had been turned off, the liquid nitrogen refrigerant was replaced by another refrigerant; a 2:1 mixture (by volume) of isopentane and 2-methylpentane precooled to the desired temperature level. This could be as low as -168°, the freezing point of the mixture. In this cryogenic inlet system the refrigerant is cooled by passing liquid nitrogen through an immersed cooling coil at a controlled rate and warmed by an immersed electric heater connected to an automatic unit[23]. This system can be maintained automatically at any desired temperature or warmed in a controlled manner. Since the inlet system is maintained at the refrigerant temperature up to the point of interaction with the ionizing electro beam, the different compounds evolving at different temperatures can be analyzed mass spectrometrically without further warm-up.

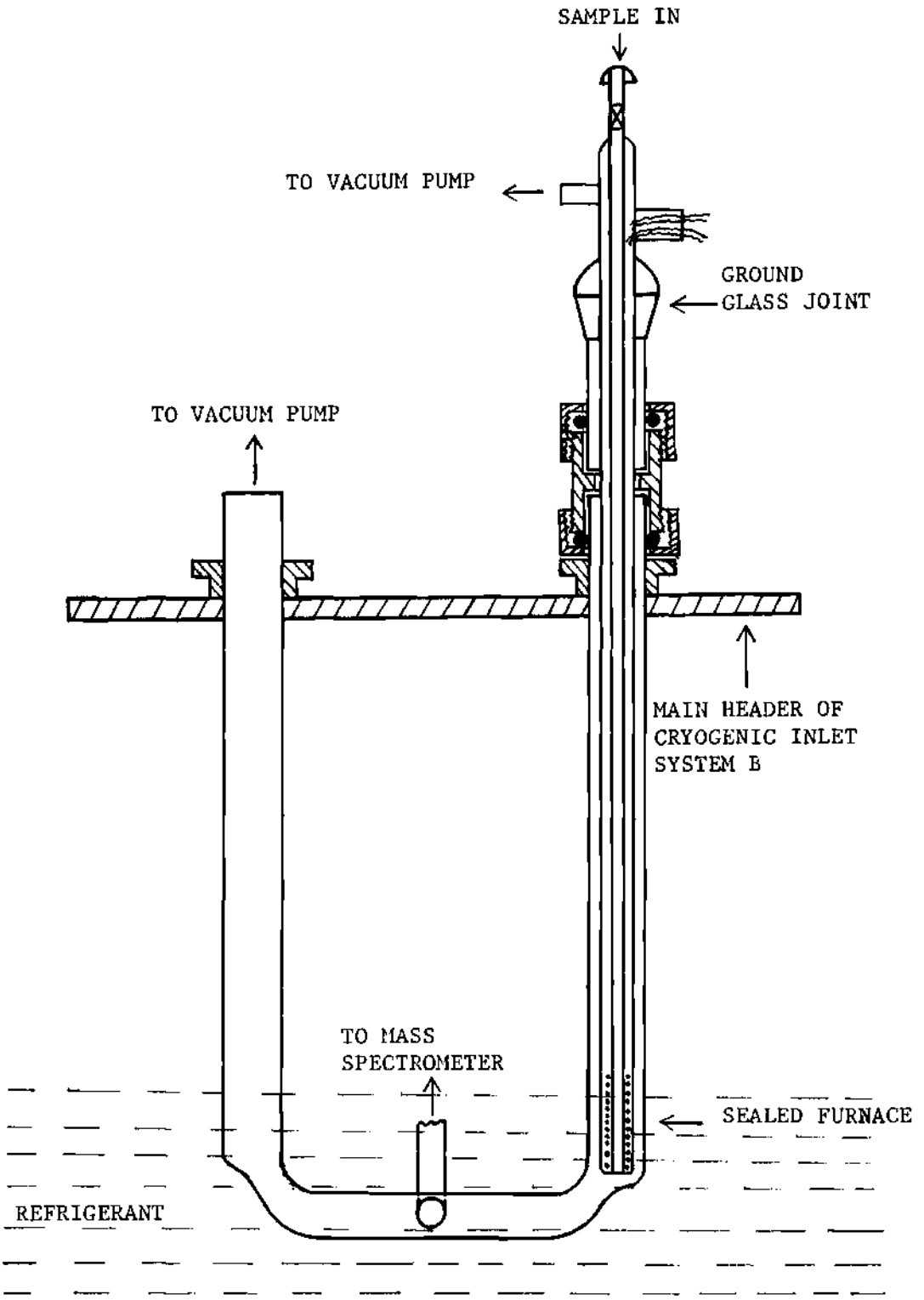

Figure 4. Sealed Furnace inside U-tube Reactor.

Chemical Preparations

Borane Carbonyl

Borane carbonyl was formed by reacting diborane with carbon monooxide under conditions as described by Burg[24]. Diborane was introduced into an evacuated 500 ml volume ICC-3B-400 Hoke sampling stainless steel cylinder up to a pressure of about 17 psia at room temperature and then carbon monooxide gas was introduced up to a total pressure of about 160 psia at room temperature. These two gases were then mixed by vigorous shaking of the cylinder which contained some polyethylene chips. The gas mixture was then heated by immersion in boiling water for about 15-20 minutes, and the cylinder was then dipped into liquid nitrogen to prevent decomposition of the BH_3CO that had been formed. Borane carbonyl was collected in pure form by low-temperature trap-to-trap distillation as described by Burg[24]. Purity of the borane carbonyl sample was determined mass spectrometrically. Small amounts of diborane may be found initially, but this can be removed by pumping through the mass spectrometer for sometime with the sample at about -158°. The purified borane carbonyl sample was stored at liquid nitrogen temperature.

Tetraborane(10)

The source of tetraborane(10) was a diborane cylinder left at room temperature for about three years. At room temperature B_2H_6 will be converted slowly to H_2, B_4H_{10} and higher boranes[19]. B_4H_{10} and higher boranes free of B_2H_6 and H_2 were collected in a trap at -140° by low temperature distillation. Higher boranes were separated in a trap at -110° and B_4H_{10} was collected in an adjacent trap at -150°. With the sample of B_4H_{10} at -120°, the mass spectrum was that of pure B_4H_{10}.

However, at -90° and above there were signs of higher boranes in the sample. During experiments with B_4H_{10} the trap was always kept below -120°. The tetraborane samples were stored at liquid nitrogen temperature.

Energy Measurements

Appearance potential measurements for parent or fragment ions were made by an electron impact method in the T-O-F mass spectrometer by measuring and comparing the ionization efficiency curves for both the unknown and standard ions.

The observed ion current (I) in a mass spectrometer is a function of the density of the electron beam (ρ_e) (which is a function of trap current), the density of the sample gas (ρ_s), the gross ionization cross section σ (eV) (which is a function of electron energy and the ion concerned), and a combined electronic factor of the instrument (K) as:

$$I = K\rho_e\rho_s\sigma(eV).$$

Assuming the other factors to be constant, the ion current should vary as the ionization cross section or, in other words, the ionization probability will vary with the electron energy. It has been verified by monoenergetic electron beam methods that for standard gases such as He, the ionization probability increases linearly with electron energy up to several electron volts above the onset of ionization. In case some other processes are also occurring which affect the ionization probability, the IE curve will be made up of a linear superposition of all the ionization probabilities due to the different processes. The possible processes leading to structure in IE curves are:

I.	For parent ions	II.	For fragment ions
A.	Autoionization	F.	Ion pair formation
B.	Excited stable ions	G.	Rearrangements
C.	Ion instabilities	H.	Ion-neutral
(i)	Metastable ions	I.	Excited neutral
(ii)	Ion-pair formation	J.	Excited ion
(iii)	Ion-neutral.	K.	Fragmentation of neutral.

Interpretation of ionization efficiency data becomes very complicated when several of these processes compete with each other. In most mass spectrometers (including the Bendix TOF MS), the ionization is produced by a beam of electrons having a thermal distribution of energies which may be approximated by quasi-Maxwellian distribution and whose magnitude depends upon the filament temperature and the nature of the filament itself. So in these cases the electrons will possess the applied electron energy plus this thermal energy. Since the high energy section of the thermal distribution is exponential, the IE curves begin with an exponential curved region of about two volts, followed by an intermediate curved region of one to two volts which passes into an apparently linear region for a few volts. The curves usually continue to increase upward until about 40 volts they typically begin to flatten out. Due to the effect of electron energy distribution as well as many other instrumental factors affecting the electron energy, to obtain an appearance potential it is necessary to compare and relate the ionization efficiency curve of an ion with the IE curve of a calibrating gas with an accurately known IP, usually a rare gas or a simple polyatomic molecule. So the main problem is now how to compare and relate the IE

curve of the desired compound with that of the calibrating gas. IE curves of the usual shape similar to that of the calibrating gases are called "standard curves" whereas some low intensity fragment ions have long tails at the initial part of their IE curves due to the occurrence of multiple processes. These "long tail curves" present a special problem in appearance potential determination.

The several mass spectrometric methods that are used at present to extract ionization potentials (IP) from the ionization efficiency (IE) curves can be grouped together as follows:

1. The vanishing current method of Smyth[25].
   a. By the vanishing point[25].
   b. By extrapolated differences, Warren[26].
2. The logarithmic methods.
   a. The critical slope method of Honig[27].
   b. The method of Lossing, Tickner, and Bryce[28].
   c. Semilogarithmic matching method of Foner and Hudson[29].
   d. The method of Dibeler and Reese[30].
3. The linear extrapolation method for experiments.
   (i) with electrons having thermal energy distribution: linear extrapolation method of Smith[31]; (ii) with mono-energetic electrons:
   a. direct, Clarke[32].
   b. by means of a retarding potential difference (R.P.D.), Fox et al[33].
4. The second derivative method of Morrison[34].

These methods with their merits and demerits have been described

in detail in several theses from this laboratory.

We used a technique which has the combined ideas of the linear extrapolation method of Smith, the vanishing current method, and the extrapolated difference method, and it was easily adapted to the X-Y recorder output presentation of our equipment. In this method the IE curves for the sample and calibrating gases are overlapped from the initial onset to about one to two volts into the linear region. This method, which can be named as "overall match" method, gives appearance potential values with an uncertainty of 0.1-0.2 eV for sufficiently well-behaved systems.

For samples exhibiting near standard IE curves, all of the above mentioned methods should determine the IP with reasonable accuracy. We decided to use mainly the "overall match" method.

It can be reasoned theoretically that RPD and second derivative methods should separate the IE curves into contributions from the various processes that occur, and thereby both should be directly applicable to long-tail ions. But practically for low intensity ions, the accuracy of both methods becomes questionable[35] unless the two separate processes are at least two eV apart. We decided to use the method of "initial break" along with the semilog match method for long-tail ions. Assuming that only one process was taking place within the first two volts above the AP, the unknown sample IE curve and the calibrating ion IE curve were matched for two volts above AP. However, this reasoning may also fail if the ion intensities are very low[36], i.e., if instrumental sensitivity limitations dominate, or if the processes are too closely spaced.

Excess Energy Measurements

The excess energies of products of unimolecular dissociations resulting from electron impact may in general be defined as the difference between the AP and the ground state heat of reaction ΔH°. When a diatomic molecule is ionized and excited to a state above one of its decomposition asymptotes, the molecular ion will dissociate into two fragments whose excess energy, $AP-\Delta H^\circ$, will be equal to the sum of their translational energies provided there is no electronic excitation. For polyatomic systems, there is no such simple relationship, because part, or all, of the excess energy can now remain in the vibrational modes of the products.

A legitimate criticism of all molecular energetic arguments based upon electron impact data concerns the possible production of excited ions. In general, the parent molecular ion contains no excess translational energy and little excess vibrational energy (< 0.2 eV). For fragment ions, however, the probability of excess energies in the form of translational, rotational, vibrational and sometimes even electronic excitation increases with the number of bonds broken.

The kinetic energy of fragment ions are measured by two types of methods: those using retarding potentials in the ion source and those based on the focusing properties of ions formed with translational energy. These methods can be adapted either to conventional magnetic mass spectrometers or to specially designed instruments. A technique of making these measurements with the T-O-F mass spectrometer has been developed by Franklin[37]. The excess translational energy, $\bar{e}_t$, measured in this way has also been correlated[38] well with the total excess energy

E* (neglecting rotational energy) as: $\bar{e}_t = \frac{E^*}{\alpha N}$ where N is the number of classical oscillators and α is an arbitrary parameter which is shown to be approximately the same for a large number of fragmentation processes involving a varied array of molecules. In this correlation the fragmentation was basically considered to be a kinetic problem and therefore the energetic quantities were related by this empirical equation whose form was suggested by previous correlations of kinetic data.

The method of determining excess energies in unimolecular dissociation resulting from electron impact in T-O-F mass spectrometer has already been described in detail[35] and so this discussion will include only a brief description of the procedure.

Procedure

1. Obtain a calibration curve relating peak width at half height, $W_{1/2}$, to the square root of the mass $\sqrt{M}$ and gate width for room temperature thermal ions; (Ion focus pulse, vertical deflection, and horizontal deflection should be so adjusted that the peaks are tallest and thinnest).

2. Obtain $W_{1/2}$ versus electron energy for each fragment ion; and correct for the effect of gate width;

3. Obtain translational energy of the fragment ion $\bar{e}_i$ at the AP by extrapolating a plot of $\bar{e}_i$ (calculated from corrected $W_{1/2}$) versus electron energy;

4. Calculate $\bar{e}_t$ at the AP from $\bar{e}_i$ by the equation:

$$\bar{e}_t = (M_i + M_n)\bar{e}_{i/M_n} - (M_i/M_n)(3/2)kT$$

where M_i and M_n are masses of the ion and neutral, respectively.

5. Calculate excess energy E* at the AP from $\bar{e}_t$ by the equation:

$$\bar{e}_t = E^*/\alpha N$$

with $\alpha = 0.44$ as developed by Franklin[37].

For low mass ions with low ion intensities and little excess energy, a three-step procedure should be used to detect the presence of excess energy. First, a large gate should be used to obtain an upper limit on the excess energy. Then a small gate should be used to also detect any excess energy. Thirdly, the two $\bar{e}_i$ versus electron energy curves should be compared and both used to determine how the curves and the extrapolation should be drawn.

CHAPTER III

RESULTS AND DISCUSSION

Pyrolysis Studies with Borane Carbonyl

Pyrolysis studies with borane carbonyl were performed in the coaxial furnace inlet system described in Chapter II. Significant decomposition of BH_3CO begins at about 220°, and with increasing temperature, the amount of BH_3CO decreases rapidly while that of B_2H_6 and BH_3 both increase up to a certain temperature depending upon the furnace design and the inlet pressure of BH_3CO. The spectra indicated a maximum yield of BH_3 when the exhaust port of the pyrolysis furnace was virtually tangent to the ionizing electron beam. Using the 4 mm i.d. x 4 cm long quartz furnace described earlier at a temperature of 250° and an input gas pressure of 55×10^{-3} torr, the spectrum that was observed is shown in Table 1. Peaks in the BH_3 region are much larger than would be possible from combined B_2H_6 and BH_3CO along. For some convenient and reasonably optimum experimental conditions, the relative amounts of BH_3CO, B_2H_6, and BH_3 were approximately 3:4:3 respectively. This suggests the presence of a large amount of free BH_3 in the pyrolysis products. With increasing temperature above 250°, the amount of diborane increases while that of both BH_3CO and BH_3 decrease due to more decomposition of BH_3CO and higher rate of reaction of BH_3 with BH_3CO. No higher boranes were observed in these pyrolysis experiments.

Ionization efficiency measurements at m/e 14 from the furnace

Table 1. Mass Spectra of the Pyrolysis Products of Borane Carbonyl at a Furnace Temperature of 250° and at an Inlet Pressure of 55×10^{-3} torr

m/e	*Relative Intensity in Spectrum of Pyrolysis Products of BH_3CO	Relative Intensity of Pure B_2H_6 Spectrum at Room Temperature	Relative Intensity of Pure BH_3CO Spectrum at Room Temperature
39	80	0	100
27	56	100	0
13	100	24	50
12	200	20	45
11	40	25	25
10	8	5.5	5

*M/e 13 was considered base 100 because it should be the main peak in the BH_3 region and also because m/e 12 has a contribution from the C^+ ion.

effluent gas yielded $I(^{11}BH_3) = 12.24 \pm 0.1$ eV. The energetics section of this chapter will discuss the comparison of the appearance potential data on B_2H_6 reported by Wilson and McGee[11] with those on BH_3CO from this work. The intermeshing consistency of data on B_2H_6 and BH_3CO strongly suggests that the measurements on BH_3 do in fact refer to that species and not to a possible excited or partially opened diborane, $B_2H_6^*$, as might be supposed[39]. Furthermore, an optimum pyrolysis temperature of 380° yielded small amounts of BH_3 from B_2H_6 while 250° resulted in large amounts of BH_3 from BH_3CO along with some unavoidable B_2H_6 contamination. Yet the minimum appearance potential of BH_3 in the pyrolysis products was the same (12.3 eV) in both experiments. The standard mass spectrum of B_2H_6 was unchanged in complex beam inlet experiments wherein there was no possibility of sample heating (usually to 250°) as is characteristic of standard sources[39]. This suggests insignificant excitation of B_2H_6 at temperatures approaching that of the BH_3CO pyrolysis. Also the temperatures of maximum BH_3 concentration in these pyrolyses were much less than the 900° reported by Stafford, et al.[39] in their concern about the presence of a possible $B_2H_6^*$. Finally, if the measured $A(BH_3^+)$ is from $B_2H_6^*$, then $I(BH_3)$ is a still smaller number and correspondingly $D(BH_3 - BH_3)$ and $D(H_3B\text{-}CO)$ would be larger than reported here. $D(BH_3 - BH_3) = 59 \frac{kcal}{mole}$ has seemed rather large already.

Pyrolysis Study with B_4H_{10}

Baylis, et al.,[3] studied the pyrolysis of $^nB_4H_{10}$ with an "integral furnace" mass spectrometer with reactor temperatures between 10° and

285° and reactor pressures of B_4H_{10} of about $10^{-5.2}$ atm. (4.8×10^{-3} torr). They found B_4H_8 as an intermediate produced in the pyrolysis.

Similar mass-spectrometric studies with $^nB_4H_{10}$ were conducted in the coaxial furnace inlet system with a sealed furnace. Room temperature mass spectra of $^nB_4H_{10}$ did not reveal any evidence of its pyrolysis in the ion source and no higher borane was formed, although the spectra differed by a small extent from the spectra[3] at 10° due to instrumental factors. The spectrum of tetraborane(10) in the B_4-region has contributions from several ions. For example, the peak at m/e 53 is due to $(^{11}B_3{}^{10}BH_{10})^+$ and $(^{11}B_4H_9)^+$ ions. Similarly, the peak at m/e 52 is due to $(^{11}B_4H_8)^+$, $(^{11}B_3{}^{10}BH_9)^+$, and $(^{11}B_2{}^{10}B_2H_{10})^+$ ions, the peak at m/e 51 is due to $(^{11}B_4H_7)^+$, $(^{11}B_3{}^{10}BH_8)^+$, $(^{11}B_2{}^{10}B_2H_9)^+$, and $(^{11}B^{10}B_3H_{10})^+$ ions; the peak at m/e 50 is due to $(^{11}B_4H_6)^+$, $(^{11}B_3{}^{10}BH_7)^+$, $(^{11}B_2{}^{10}B_2H_8)^+$, $(^{11}B^{10}B_3H_9)^+$, and $(^{10}B_4H_{10})^+$ ions; the peak at m/e 49 is due to $(^{11}B_4H_5)^+$, $(^{11}B_3{}^{10}BH_6)^+$, $(^{11}B_2{}^{10}B_2H_7)^+$, $(^{11}B^{10}B_3H_8)^+$, and $(^{10}B_4H_9)^+$ ions; and the peak at m/e 48 is due to $(^{11}B_4H_4)^+$, $(^{11}B_3{}^{10}BH_5)^+$, $(^{11}B_2{}^{10}B_2H_6)^+$, $(^{11}B^{10}B_3H_7)^+$, and $(^{10}B_4H_8)^+$ ions. The change of tetraborane spectrum with temperature was similar to that in the stydy of Baylis, *et al.*,[3] and the presence of B_4H_8 was confirmed in the same way by observing the increase in the ion intensity ratios of $I(48^+)/I(50^+)$, $I(49^+)/I(50^+)$, and $I(52^+)/I(53^+)$. The relative intensity of the peaks at m/e 48 and m/e 49 (relative to m/e 50 = 100%) increases starting at 70° to a maximum value at 250° when a decrease in the ratio can first be observed. There is a large decrease in the relative intensity of m/e 53 from 70° through 230°. The relative intensity of m/e 52, however, increases in this same temperature region. Consequently, the ratio

$I(52^+)/I(53^+)$ increases with temperature until 230°. In the pyrolysis of B_4H_{10} at a temperature of 250° and at a B_4H_{10} pressure of about 5×10^{-3} torr, the observed spectrum appears to show a maximum percentage of B_4H_8. Small amounts of higher boranes and diborane were also observed, but their amount was so small that the spectrum in the B_4-region would not be appreciably affected.

Cryosynthesis of Borane

Pyrolysis and rapid quenching experiments of borane carbonyl were conducted in the cryogenic reactor inlet system A maintained at 65°-67°K as described earlier and using a sealed furnace. Refrigeration capacities limited experiments to about 40 minutes duration with furnace inlet pressures of BH_3CO of 1 to 100 x 10^{-3} torr and temperatures of 280° to 350°. During these experiments BH_3, B_2H_6, and CO were observed as having passed completely through the quenching space. For such observation, the furnace effluent must pass through a tubular quenching space 1/2 in i.d. x 4 1/8 in long and a 1/8 in i.d. x 1 1/8 in long tube all at 67°K before emerging into the ion source at a point 3/8 in from the ionizing electron beam to yield mass spectra like that of Table 2. After the pyrolysis was completed and the furnace had been turned off, the quenching space could be maintained at 65°K for about 16 minutes, during which time BH_3, B_2H_6, and small amounts of CO were continually observed in spectra like that of Table 2. As the quench reactor then slowly warmed up from 65°K, the spectra gradually became that of authentic B_2H_6, and BH_3CO was observed above 90°K. This total sequence of observations was repeated in three separate experiments.

Table 2. Relative Intensities of BH_n^+ Ions for B_2H_6 and for the Equilibrium Vapor over the Cold Composite Solid from the Pyrolysis and Quench of BH_3CO

m/e	T = 65°K	T = 67°K	Diborane at 90°k
27	100	100	100
13	72	35.5	19.5
12	44	47.5	14.5
11	26.6	21	18.7
10	6	5	4.1

Diborane has insufficient vapor pressure at 65°-67°K to be detectable in this cryogenic mass spectrometric inlet system. At sufficiently high temperatures to be seen, authentic B_2H_6 is characterized by an m/e 13 to m/e 27 ratio of 0.2 as shown in Table 2. In these experiments, not only is B_2H_6 seen, but the 13/27 ratio is 0.35 to 0.6 at 67°K and 0.7 to 0.8 at 65°K. We conclude that free BH_3 survives both transport through the quench-reactor and condensation and revaporisation at 65°-67°K, and that the observed low temperature spectra are due to free BH_3 and B_2H_6 formed by recombination in the quench reactor and in the ion source (which is at room temperature). The activation energy for recombination thus seems very low, and hence, the isolation of pure BH_3, as a useful cryogenic reagent unfortunately seems not very probable.

Cryosynthesis of Tetraborane (8)

Pyrolysis and quenching experiments with B_4H_{10} were conducted in a sealed furnace at temperatures of 220° to 250° with inlet pressure near 5×10^{-3} torr, and the furnace effluent was quenched to 77°K in cryogenic inlet system B. During the pyrolysis and quench experiments no pyrolysis products escaped the quench reactor to be detected by the mass spectrometer. Upon suddenly warming the system from 77°K to about -164° using a 2-methylpentane-isopentane mixture as refrigerant, diborane was evolved from the cryogenic reactor. At a temperature of about -135° to -110°, structure was observed in the B_4-region which had the feature of enhanced peaks at m/e 48, 49 and some other changes relative to the B_4H_{10} spectrum (Table 3) at -110°. At -124° the spectrum of the quenched product was as given in Table 3. These observations were reproduced

Table 3. Relative Intensities of Ions in the B_4 Region for B_4H_{10} and for the Equilibrium Vapor over the Cold Composite Solid from the Pyrolysis and Quench of B_4H_{10}

m/e	B_4H_{10} at -110°	Quenched Product at -124°
52	12	11
51	26.5	25
50	100	100
49	84.5	99.5
48	72	80
47	54	61
46	41.5	44.5
45	26.5	29.5

three times. The spectrum of B_4H_{10} at -110° without pyrolysis (Table 3) was reproduced several times, but it never showed any enhancement at m/e 48, 49 or any other changes in the spectrum as were seen in the pyrolysis experiments and also in the pyrolysis and quench experiments with B_4H_{10}. This result suggests that the spectrum of the quenched pyrolysis products at -124° is due to B_4H_{10} and B_4H_8 and that B_4H_8 must have survived quench and revaporization. But the vapor pressures of B_4H_{10} and B_4H_8 are too similar to allow a separation of these B_4 species by simple distillation a one at very low temperatures. Higher boranes in the B_5, B_6, and B_7 region were observed at temperatures above -95°. The spectrum of the quenched pyrolysis product at -124° did not show any strong evidence of decomposition of B_4H_8 or of its reaction either with itself or with B_4H_{10}.

Molecular Energetics of Borane Carbonyl

Ionization efficiency measurements at m/e 14 from the furnace effluent gas yielded $I(^{11}BH_3) = 12.24 \pm 0.1$ eV using the extrapolated difference method[26] from "overall matched" IE curves on fifteen independent sets of data. Appearance potentials of the fragment ions from BH_3CO were also determined by the same extrapolated difference method. In these measurements a precision of ± 0.2 eV was obtained from typically nine independent sets of data. All these measured appearance potential values together with those of the BH_3 - B_2H_6 system reported by Wilson and McGee[11] are presented in Table 4. These numbers permit a complete development of the molecular energetics of BH_3CO which will now be discussed. Representative ionization efficiency curves obtained in this

Table 4. Appearance Potentials of Fragment Ions from BH_3, B_2H_6, and BH_3CO

Fragment Ion	Appearance Potential from Parent (eV)		
	BH_3[a]	B_2H_6[a]	BH_3CO[b]
10_B^+	15.83[c]	18.39 ± 0.02	19.31 ± 0.2
10_{BH}^+	13.66 ± 0.02	16.39 ± 0.3	15.16 ± 0.2
$10_{BH_2}^+$	12.95 ± 0.05	15.50 ± 0.05	14.36 ± 0.2
$11_{BH_3}^+$	12.32 ± 0.1	14.88 ± 0.05	13.70 ± 0.2
	12.24 ± 0.1[b]		

[a]Values from Ref. 11.

[b]This work.

[c]Value calculated in Ref. 11.

work are presented in Appendix B.

$D(BH_3\text{-}CO)$

The four measured appearance potentials of fragment ions from BH_3CO in Table 4 together with the corresponding data from the fragmentation and ionization of BH_3 permit four independent determinations of the bond dissociation energy, $D(BH_3\text{-}CO)$. For the process

$$e + BH_3CO \rightarrow BH_3^+ + CO + 2e, \qquad (1)$$

$A(BH_3^+) = D(BH_3 - CO) + I(BH_3)$, or $D(BH_3 - CO) = 13.70 - 12.24 = 1.46$ eV. Similarly for the process

$$e + BH_3CO \rightarrow BH_2^+ + H + CO + 2e, \qquad (2)$$

$A(BH_2^+) = D(BH_3 - CO) + D(BH_2 - H) + I(BH_2)$. But these last two terms are just $A(BH_2^+)$ from BH_3, and one can write, $D(BH_3 - CO) = 14.36 - 12.95 = 1.41$ eV. Similarly, with $A(BH^+)$ and $A(B^+)$ one obtains $D(BH_3 - CO) = 1.50$ and 3.51 eV, respectively. With the exception of the last value, there is excellent agreement, and $D(BH_3 - CO) = 1.46$ eV or 33.7 kcal/mole seems well established. We shall discuss the apparent inflated value of $A(B^+)$ from BH_3CO subsequently.

Internal Consistency

Convincing checks of the consistency of the data on BH_3CO, B_2H_6, and BH_3 that appear in Table 4 can be developed. For example, in Process (2), $A(BH_2^+) = A(BH_3^+) + D(BH_2^+ - H)$, or $D(BH_2^+ - H) = 14.36 - 13.70 = 0.66$ eV, while the similar processes with BH_3 and B_2H_6 yield $D(BH_2^+ - H) = 0.63$ and 0.62 eV, respectively. The similar process and calculation,

but involving the appearance of BH^+, yielded $D(BH^+ - H) = 0.80$, 0.71, and 0.89 eV, respectively. The appearance of B^+ yielded $D(B^+ - H) =$ 4.15, 2.14, and 2.00 eV, respectively, which is not too informative since $A(B^+)$ from BH_3 was not measured,[11] but the apparent inflated value of $A(B^+)$ from BH_3CO is again evident.

If we assume $D(BH_3 - CO) = 33.7$ kcal/mole as developed above to be correct, one can calculate the heat of atomization of BH_3 from

$$\Delta H_f(BH_3CO) = \Delta H_{sub}\ (B) + 3\Delta H_f(H) + \Delta H_f(CO) - D(BH_3 - CO) - [D(BH_2 - H) + D(BH - H) + D(B - H)].$$

This yields

$$D(BH_2 - H) + D(BH - H) + D(B - H) = 27.24 + 134 + 3(52.1) - 26.42 - 33.7 = 257.5 \text{ kcal/mole}.$$

A similar calculation with data on B_2H_6 yields 256.5 kcal/mole[11].

$D(BH_3 - BH_3)$

The above calculation of the heat of atomization of BH_3 from B_2H_6 employed $D(BH_3 - BH_3) = 59$ kcal/mole,[11] and hence the indicated agreement suggests consistency as regards $D(BH_3 - BH_3)$ between the B_2H_6 and the BH_3CO data. In addition, equilibrium data observed in the range 25° - 80° for the reaction,

$$2BH_3CO \rightleftarrows B_2H_6 + 2CO, \qquad (3)$$

may be fitted by $\Delta G = \Delta H - T\Delta S = 9.142 - T(0.0325)$ kcal/mole[16]. Using $\Delta H = 9.142$ kcal/mole for the above reaction and $D(BH_3 - CO) = 33.7$ kcal/mole, one deduces $D(BH_3 - BH_3) = 58$ kcal/mole which represents still another independent confirmation of the magnitude of the symmetric dissociation energy of diborane.

$\underline{A(B^+)}$

The large measured value of $A(B^+)$ from BH_3CO is puzzling. For the process

$$e + BH_3CO \rightarrow B^+ + H_2 + H + CO + 2e, \qquad (4)$$

$$A(B^+) = D(BH_3 - CO) + \Delta H_{atom}(BH_3) + I(B) - D(H - H)$$

or

$$\Delta H_{atom}(BH_3) = 19.3 - 1.46 - 8.3 + 4.52 = 14 \text{ eV} = 324 \text{ kcal/mole}.$$

This result is 67 kcal/mole higher than the 257 kcal/mole calculated above. Evidently some process other than (4) is occurring. A similar calculation with $A(B^+)$ from B_2H_6 gave $\Delta H_{atom}(BH_3)$ that was 1.0 eV too high, but this excess energy could reasonably be assigned to product H_2 appearing with 2 quanta of vibrational excitation[11]. If we make this same assignment in Process (4), we must also assign 1.9 eV or 8 quanta of vibrational excitation to product CO. No CO excitation would suggest $A(B^+)$ should be about 17.4 eV which would make the difference in the appearance potentials from BH_3CO and B_2H_6 of each ion in Table 4 identical to each other to well within experimental error. This equivalence is, of course, expected. Certainly the onset of significant cross sections for collisions producing products in closely spaced internal

states will yield ionization efficiency data that can be easily misinterpreted. Some progress with such problems has occurred[34]. As has been similarly noted for hydrocarbons,[36] too low an ion concentration may also be the cause of the high value of $A(B^+)$ due to the now greatly enhanced importance of instrumental sensitivity.

It is entirely possible that $A(BH^+) < A(BH_2^+)$ due to H_2 formation with BH^+ which would suggest that $A(^{10}BH_2^+)$ of Table 4 is actually $A(^{11}BH^+)$. However, this assumption leads to unreasonable energetic consequences, and it does not explain all the data.

The notion of one or more excited products is the simplest, though not definitive, explanation of the large value of $A(B^+)$.

Excess Energy Measurements

A legitimate criticism of all molecular energetic arguments based upon electron impact data concerns the possible production of excited ions. To resolve this uncertainty, excess energy measurement experiments were conducted in search of a possible excited BH_3^+ ion in the dissociative ionization of B_2H_6. If excitation had occurred in the appearance of BH_3 from B_2H_6, the observed AP would have exceeded the true value by the amount of this excitation, and the deduced value of $D(BH_3 - BH_3)$ would have been correspondingly too large by this same amount. As discussed earlier, in dissociative ionization, the total excess energy of an ion has been shown to correlate well with its translational excitation,[38] and the latter is readily determined from measurements of peak widths at half-height, $W_{1/2}$, as a function of electron energy[37]. In the appearance of $^{11}BH_3^+$ ion from B_2H_6, these measurements were made at a series of electron energies and at different gate

widths as shown in Tables 5 and 6. Similar measurements were also made for the parent ions of He, H_2O, N_2, and Ar as shown in Tables 5 and 6 which are known to be produced with no excess translational energy. By comparing the peak widths at half-height, $W_{1/2}$, given in Table 4 and 5 for $^{11}BH_3^+$ and other ions it can be seen that $^{11}BH_3^+$ ion does not have any extra broadening of the peak width which would have been caused by excess translational energy. If the BH_3^+ ion had had translation excitation, then its $W_{1/2}$ values would be much larger than that of H_2O^+ ions. The $W_{1/2}$ data for BH_3^+ vary from 65 mm to 86 mm and below 30 eV they do not exceed 70 mm; the $W_{1/2}$ value for H_2O^+ ion at 70 eV is about 76 mm. This comparison shows that the BH_3^+ ion does not have any translational excitation. So the excess energy of $^{11}BH_3^+$ ion at its appearance potential from B_2H_6 is zero. The absence of excitation in $^{11}BH_3^+$ ion from B_2H_6 further supports our energetic arguments.

Molecular Energetics of Some B-H-F Compounds Using the MINDO Method

To further authenticate these energetic arguments from a theoretical perspective, the new MINDO molecular orbital method[40] has been calibrated for B-H and B-F bonds. The MINDO method was selected because of its demonstrated superior accuracy in calculations of heat of formation and ionization potentials for a wide variety of compounds. The MINDO method will be described in Appendix A. The program used here was obtained from the Quantum Chemistry Program Exchange, Chemistry Department, University of Indiana, Bloomington, and was designated MINDO 4. The heat of formation of the fluorine atom was changed to 15.45 kcal/mole[41] rather than 18.86 kcal/mole. In the MINDO approximation,

Table 5. Peak Width at Half-Height Data at Gate Width of 4.5

Ion	Electron Energy, eV.	$W_{1/2}$ mm. (Uncorrected)
Ar^+	70	85
O_2^+	70	81
N_2^+	70	80
H_2O^+	70	75
He^+	70	65
BH_3^+ from B_2H_6	70	81
	50	81
	40	73
	30	70
	25	70
	20	67
	19	66.5
	18	66
	17	66
	16	66

Table 6. Peak Width at Half-Height Data at Gate Width of 5

Ion	Electron Energy, eV.	$W_{1/2}$ mm. (Uncorrected)
O_2^+	70	81
N_2^+	70	80
H_2O^+	70	76
He^+	70	65
BH_3^+ from B_2H_6	70	86
	50	84
	40	84
	30	71
	25	70
	20	70
	19	70
	18	70
	17	70
	16	70

the one-center repulsion integrals are written in terms of the Slater-Condon parameters which, along with the one-center attraction integrals, are input data and are listed in the program as a block data subroutine. The MINDO approximation for the one-electron resonance integral is:

$$\beta_{\mu\nu} = S_{\mu\nu} \left(I_{\mu} + I_{\nu}\right) \left(\beta^{I}_{AB} + \beta^{II}_{AB}/R^{2}_{AB}\right)$$

where Φ_{μ} and Φ_{ν} are atomic orbitals of atoms A and B respectively, I_{μ} and I_{ν} are the corresponding valence state ionization potentials, $S_{\mu\nu}$ is the overlap integral, R_{AB} is the internuclear separation of the atoms, and β^{I}_{AB} and β^{II}_{AB} are empirical parameters for A-B type bonds which we must now evaluate for B-H and B-F bonds. This was accomplished for B-H by temporarily setting $\beta^{II}_{BH} = 0$, setting R_{BH} of single bonded BH equal to the measured value of 1.2325 Å[42], and evaluating β^{I}_{BH} by fitting $\Delta H_f(BH) = 104$ kcal/mole[43]. In the MINDO method, standard bond lengths rather than experimental values are used, but these values were not significantly different from the actual ones for small hydrocarbons, and hence the experimental R_{BH} was used. The resulting value of β^{I}_{BH} and using $R_{BH} = 1.19$ Å[44] in sp^2 hybridized BH_3 permitted a computation of the $\Delta H_{atom}(BH_3) = 256$ kcal/mole which is in very good agreement with the electron impact based value of 257 kcal/mole. Since BH and BH_3 have different kinds of bonds, β^{II}_{BH} was given a value greater than zero, and then both β^{I}_{BH} and β^{II}_{BH} were adjusted to obtain an optimum consistency for both BH and BH_3 (see Tables 7 and 8). Calibrating on larger values of $\Delta H_f(BH)$, but within the experimental uncertainty, yields values of $\Delta H_{atom}(BH_3)$ somewhat smaller than 257 kcal/mole, for example, at ΔH_f = (BH) = 106 kcal/mole, $\Delta H_{atom}(BH_3)$ is computed to be 250 kcal/mole. Thus,

to achieve optimum consistency the MINDO computation permits a selection of heat of formation data from within the stated experimental uncertainties. A change in bond length in BH_3 of 0.01 Å still yields energetic quantities within the experimental uncertainties.

We have been unsuccessful in applying the MINDO technique to the three-center-two-electron bonds of B_2H_6.

It is instructive to inquire whether the parameters which correlate our experimental results on BH and BH_3 will correctly predict the heat of formation of BHF_2. Since BHF_2 has the same sp^2 hybrid B-H bond as found in BH_3, a "standard" bond length of 1.19 Å was used for the calculation. The parameters for the sp^2 hybridized B-F bond were obtained by setting R_{BF} = 1.3 Å, the experimental value in BF_3,[45] and evaluating β_{BF}^{I} by fitting $\Delta H_f(BF_3)$ (see Tables 7 and 8). β_{BF}^{II} was set equal to zero since all of the compounds considered here have the same kind of B-F bond, and a "standard" bond length was used. One then calculates $I(BF_3)$ = 15.45 eV which may be compared with $I(BF_3)$ = 15.55 ± 0.04 eV from photoionization experiments,[46,47] and $\Delta H_f(BHF_2)$ =-176.805 kcal/mole, which may be compared with an experimental value of -175.7 ± 1.5 kcal/mole,[48] and $I(BHF_2)$ = 13.80 eV for which there is no experimental value.

These parameters were also used to calculate $\Delta H_f(BF)$ and I(BF). The assumption of a two-electron bond and the use of the measured bond distance of 1.265 Å[49] yields poor agreement with experiment. However, use of an sp^2 hybrid bond,[50] and a "standard" bond length of 1.3 Å as in BF_3, yields very good agreement with experiment, as is evident from Table 7. The theoretical I(BF) is about 0.7 eV higher than the median experimental value, but this latter value is questionable since it was

measured at about 1300°[51].

No data are available on the final member of the family, BH_2F, since it has not yet been synthesized, but MINDO predicts $\Delta H_f(BH_2F)$ = -70.6 kcal/mole and $I(BH_2F)$ = 12.08 eV. The molecules BH_3 and BH_2F are the lowest energy configurations of the four atoms. The next lowest potential minimum is 72.3 kcal/mole higher for BH_3 and 99.6 kcal/mole higher for BH_2F, hence we conclude that BH_2F is the more stable species, and if the kinetic characteristics of the fluoride are not too unlike those of BH_3, we expect BH_2F to be synthesizable if perhaps only at very low temperatures.

A thorough study of the efficacy of the MINDO method with B-H-F compounds is limited by the small number of compounds with no three-center-two-electron bonds.

Energetics of B_2H_6 and BH_3CO. The heat of atomization of BH_3 is 256.5 kcal/mole and 257.5 kcal/mole from completely independent sets of data measured in our laboratory on B_2H_6 ($D(BH_3 - BH_3)$ = 59 kcal/mole) and BH_3CO ($D(BH_3 - CO)$ = 33.7 kcal/mole) respectively. In both calculations only the values of $D(BH_3 - BH_3)$ and $D(BH_3 - CO)$ are significantly questionable, as is evident from $\Delta H_{atom}(BH_3) = \Delta H_f(B) + 3\Delta H_f(H) + \Delta H_f(CO) - \Delta H_f(BH_3CO) - D(BH_3 - CO)$. Other experimental techniques have yielded $D(BH_3 - CO)$ = 23.1 kcal/mole[7] and $D(BH_3 - BH_3)$ = 35 kcal/mole,[17] both of which values yield a heat of atomization of BH_3 of about 269 kcal/mole. Using R_{BH} = 1.19 Å, a value of β^I fit to 269 kcal/mole, and $\beta^{II} = 0$, $\Delta H_f(BH)$ is calculated to be 100.5 kcal/mole which is outside of the experimental range. Non-zero values of β^{II} yield even poorer agreement.

MINDO underestimated the adiabatic ionization potential of BH by only 0.06 eV (see Table 7). The difference between the calculated (11.92 eV) and the electron impact (12.24 ± 0.1 eV) ionization potential of BH_3 can be attributed to the difference between the adiabatic and vertical ionization potentials of the molecule.

All of the above suggests that viewed through the lens of the MINDO approximation there is a consistency in our earlier energetic arguments that cannot be developed using other data. The successful application of MINDO to these B-H-F compounds demonstrates the broader applicability of the method.

Table 7. A Comparison of Theoretical and Experimental Heats of Formation and Ionization Potentials

Molecule	ΔH_f(kcal/mole) Theoretical[a]	ΔH_f(kcal/mole) Experimental	IP (eV) Theoretical[a]	IP (eV) Experimental
BH	104.028	106 ± 2[b]	9.71	9.77[g]
BH_3	35.964	34.5 ± 2[c]	11.92	12.24 ± 0.1[c]
BF	-26.915	-29.0 ± 2.6[d]	12.19	11.5 ± 0.4[h]
BF_3	-270.513	-270.10± 0.24[e]	15.45	15.55 ± 0.04[i]
BHF_2	-176.805	-175.7 ± 1.5[f]	13.80	
BH_2F	-70.614		12.08	

a This MINDO calculation

b Reference 43

c Reference 11 and this work

d Reference 52

e Reference 53

f Reference 48

g Reference 54

h Reference 51

i Reference 46

Table 8. Summary of Bond Lengths and Optimum β Parameters for the Calculation of One-Electron Resonance Integrals

Molecule	Bond	Standard Bond Length (Å)	β_{AB}^{I}	β_{AB}^{II}	Bond Type
BH	B-H	1.2325	0.1765	0.005	single
BH_3	B-H	1.19	0.1765	0.005	sp^2 - hybrid
BF	B-F	1.30	0.2495	0	sp^2 - hybrid
BF_3	B-F	1.30	0.2495	0	sp^2 - hybrid
HBF_2, and	B-H	1.19	0.1765	0.005	sp^2 - hybrid
H_2BF	B-F	1.30	0.2495	0	sp^2 - hybrid

CHAPTER IV

CONCLUSIONS AND RECOMMENDATIONS

The work described in the preceeding chapters has led to the following conclusions:

(1) Large concentrations of borane, BH_3, are produced upon the pyrolysis of borane carbonyl in a coaxial furnace inlet system.

(2) Borane from the pyrolysis of borane carbonyl survives quenching to 65°-67°K and revaporization, but its isolation as a stable cryoreagent is unlikely since it dimerizes at temperatures corresponding to vapor pressures of about 5×10^{-6} torr. This suggests that borane is stable at low temperature but highly reactive with itself.

(3) The reaction intermediate B_4H_8 produced in the pyrolysis of B_4H_{10} also survives a cryogenic quench at 77°K and revaporization, but the vapor pressures of B_4H_8 and B_4H_{10} are too similar to allow a separation of these B_4 species by simple distillation alone at very low temperatures. The lack of evidence of decomposition of B_4H_8 or of its reaction either with itself or with B_4H_{10} at low temperatures suggests its stability and nonreactivity under those conditions.

(4) Ionization efficiency measurements using a fast inlet mass-spectrometric technique, have led to $I(BH_3)$ as well as $A(B^+)$, $A(BH^+)$, $A(BH_2^+)$, and $A(BH_3^+)$ from BH_3CO. These numbers, together with the appearance potential values for BH_3 system reported by Wilson and McGee[11] permit a complete development of the molecular energetics of BH_3CO. The

value of $D(BH_3 - CO) = 33.7$ kcal/mole was established which combined with earlier equilibrium data on the BH_3CO decomposition confirm $D(BH_3 - BH_3) = 59$ kcal/mole. There is an intermeshing consistency of data on both the BH_3CO and B_2H_6 systems.

(5) The MINDO molecular orbital method has been successfully applied to some B-H-F compounds which demonstrates the broader applicability of the method. Computed results by this MINDO method suggest that there is a consistency in our experimental energetic arguments that cannot be developed using other data[7,17].

(6) Experimental determination of the absence of excitation energy in the appearance of $^{11}BH_3^+$ ion from B_2H_6 supports the experimental energetic arguments on BH_3, BH_3CO, and B_2H_6.

Several extensions of the present work may be recommended.

(1) Borane from the pyrolysis of borane carbonyl should be quenched at a temperature lower than 65°K or transferred to another chamber at a lower temperature after quenching at 65°K, and then the solid quenched product should be analyzed and kept for a long period of time and analyzed later to find out if borane dimerizes in the solid phase at that low temperature and if so how quickly it dimerizes. However, during the transfer operation from one chamber to the other some amount of borane will dimerize. If borane does not dimerize in the solid phase then this solid phase should be used for low temperature spectroscopic studies of the properties of borane. If it dimerizes in the solid phase at a rapid rate then the low temperature spectroscopic studies should be made after matrix isolation. The low temperature reactivity of borane in any phase with respect to other compounds should also be studied.

(2) B_4H_8 should be obtained from a more convenient source, e.g., from the pyrolysis of B_4H_8CO[20] and then quenched and isolated by distillation. This carbonyl is, however, difficult to make. With the B_4H_8 in hand, one should then study its different chemical and physical properties.

PART II

GENERAL THEORETICAL REACTION KINETICS

CHAPTER I

INTRODUCTION

Problem Definition and Purpose

To study the cryogenic synthesis of an unknown or relatively unknown compound, it would be extremely useful if one could make some remarks, from a theoretical standpoint, on the probable existence of such compounds as stable cryochemical reagents. Suppose the desired compound is produced in some phase by some technique and then quenched at a very low temperature, then the question is whether or not it will survive under these conditions. For this purpose, it is necessary to know the stability and chemical reactivity of such compounds at low temperature. Here, chemical reactivity refers to the capacity of the molecule to react with another molecule of any kind; stability refers to the total energy of the molecule with respect to its other configurations. By the study of stability and chemical reactivity one should also be able to comment on the probability of the synthesis in general of such compounds.

Recently, some molecular orbital methods[40,55,56,57] have been developed by which one can calculate the geometry and heats of formation for some classes of compounds, and sometimes even the activation energy[56] of a reaction with more or less reasonable accuracy. In the present study of stability and chemical reactivity of cryogenic compounds, these methods will be utilized with reasonable assumptions.

To study the cryogenic stability of an unknown compound, say AJ_3,

we need to determine using MO methods first the most stable geometry of this molecule and also the relative thermodynamic stability of the molecule compared to different combinations of these four atoms, i.e., its isomers. If the desired AJ_3 molecule has the most stable configuration, its relative thermodynamic stability should be compared with that of a similar known compound to obtain more insight into its stability provided the kinetic factors in both cases may be taken as reasonably equivalent. In this case when AJ_3 is the most stable arrangement of its four atoms the next step in the determination of its cryogenic existence will be to determine its chemical reactivity or kinetic characteristics in order to determine whether or not it will react even at cryogenic temperatures. If the compound is highly reactive then in most cases it will react with itself to give less reactive products. This suggests that we need to study the general theoretical bimolecular reaction kinetics at cryogenic temperatures as a first step.

In the case where AJ_3 is unstable with respect to other combinations of these four atoms, there is the possibility of isomerization or unimolecular decomposition in addition to its being chemically reactive with itself. In this case, we need to study also the general theoretical reaction kinetics of unimolecular decomposition and isomerization at cryogenic temperatures.

The general theoretical reaction kinetics mentioned above will be studied for gas phase reactions and later an attempt will be made to correlate these results with those for similar reactions in the liquid phase.

The above discussion suggests a general approach to study the useful

existence of an unknown or relatively unknown compound at cryogenic temperatures. The remainder of this thesis will be concerned with some detailed and specific discussions of this general approach. For bimolecular gas phase reactions at cryogenic temperatures a reaction model with a relatively loose activated complex structure will be proposed. Reaction cross-sections for this model will be derived using Marcus' "Statistical-dynamical model"[59]. The expression for reaction cross-section will be used to derive finally the specific rate constant for the reaction model. Low-temperature reaction models for unimolecular reactions will be proposed and earlier developed expressions for specific rate constants will be suggested for use.

Two newly developed molecular orbital methods, the INDO[55] and the MINDO[56], will be suggested for use in the computations of the reaction characteristics of the above mentioned reactions. The use of these methods for computation of low-temperature reaction characteristics will be justified. Using a molecular orbital method, the INDO, some characteristics of the reaction of borane with borane will be studied in an attempt to justify the proposed reaction kinetic method.

Literature Review

In our discussion on general theoretical reaction kinetics, two recently developed molecular orbital methods will be used for computation purposes.

The INDO (intermediate neglect of differential overlap) MO method developed by Pople, et al.,[55] is an approximate LCAO self-consistent-field method for the determination of molecular orbitals for all valence

electrons of a molecule. This method features neglect of differential overlap in all electron-interaction integrals except those involving one center only. The parameters involved in the calculation are generally obtained semi-empirically. This method is known as the Intermediate Neglect of Differential Overlap method, and may be regarded as an improvement over the Complete Neglect of Differential Overlap or CNDO method[37]. The INDO method has been shown to yield reasonably good results in computing geometrics, particularly the bond angles for molecules, free radicals, and charged molecules by computing the minimum total energy configuration. With the input of molecular geometry, multiplicity, and charge into the INDO computer program, the total energy, electronic energy, binding energy, overlap integral matrix, columb integral matrix, core Hamiltonian, Hartree-Fock energy matrix, eigenvalues and eigenvectors, charge density matrix, and dipole moments may all be calculated for molecules composed of first row atoms.

Dewar, et al.,[40] modified the INDO method and has chosen parameters in such a way as to calculate out heats of formation and other ground state properties rather than reproducing the result that would be given by exact Hartree-Fock calculations. In this modification, as done by Dewar, et al., the various integrals were estimated in a manner similar to that used in the π approximation, the parameters being chosen to fit the observed heats of formation of selected molecules. To distinguish this treatment from INDO, it has been termed the MINDO/1 or (modified INDO) method. However, in this method one needs to use standard geometry and energetically calibrated one-electron resonance integral parameters

for a particular group of compounds. At the present state of development, this method can be used for hydrocarbons and for some limited compounds containing B, N, O, F, and H atoms. Later Dewar, et al.,[56] made an extension of this method. They wrote a computer program for automatically optimizing the parameters in MO treatments. Using this, and using parametric functions for the core resonance integrals and core-core repulsions similar to those used in the PNDO approximation, they developed a version (MINDO/2) of the MINDO method which gives good estimates of bond lengths, heats of formation, and force constants simultaneously for a wide variety of hydrocarbons only at its present state of development. Thus, the method satisfies the minimum requirements for a procedure to be used convincingly for calculating potential surfaces and activation energies for reaction. Both MINDO/1 and MINDO/2 methods give good estimates of first ionization potentials.

Both the INDO and MINDO methods and their uses have been discussed in more detail in Appendix A.

The computer programs for CNDO, INDO, and MINDO methods were obtained from the Quantum Chemistry Program Exchange, Chemistry Department, University of Indiana.

Marcus[58] gave a quasiequilibrium expression relating sums over reaction cross section to properties of activated complexes. This theory will be discussed in some detail in Appendix C. To test the quasiequilibrium assumption, Marcus applied it to recent classical-mechanical computer data on the $H + H_2$ reaction and found reasonable agreement over the range considered. Later[59] he used the quasiequilibrium expression to formulate a statistical dynamical model for total chemical-reaction cross sections

as a function of the relative velocity and the vibrational and rotational state of the reactants. It was derived for reactions for which activated-complex configurations could be defined and reactions can be with or without steric and activation barriers. A quasiequilibrium is postulated between reacting pairs and activated complexes of the same energy and angular momentum. An integral equation is obtained which is solved for the reaction cross section by introduction of a second postulate: The reaction probability is a function of the excess initial energy along the reaction coordinate (in excess of potential energy barrier, centrifugal potential barrier, and vibrational adiabatic requirements).

Marcus[59] applied his statistical-dynamical model formulations to the $H + H_2 \rightarrow H_2 + H$ reaction and compared with the exact three-dimensional classical mechanical computer calculations of reaction cross sections. Encouraging agreement was obtained in the low-to-moderate relative velocity range, without the use of adjustable parameters. At very high velocities the comparison indicates the occurrence of some vibrational nonadiabaticity.

No theoretical or experimental reaction kinetics work at cryogenic temperatures has been previously reported.

CHAPTER II

DEVELOPMENT OF GENERAL THEORETICAL REACTION KINETICS AT CRYOGENIC TEMPERATURES

To understand the cryogenic existence of a compound at low temperature, one has to know its chemical reactivity and stability.

If the compound is highly reactive, it will react with itself to give less reactive products. In this case, one should study the bimolecular reaction characteristics of the compound at low temperature. For example, there might be an exothermic dimerization reaction with reaction coordinate versus energy characteristics as shown below:

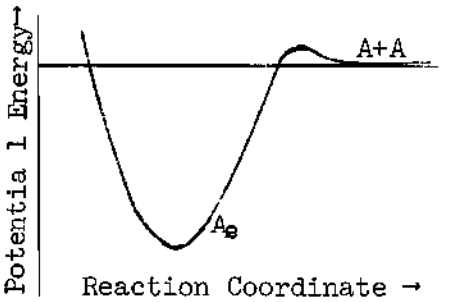

If the compound is highly unstable, then there might be an exothermic unimolecular decomposition or isomerisation reaction. In this case, it is necessary to study unimolecular decomposition reactions at low temperature having reaction characteristics as shown below, and/or isomerisation reactions at low temperature having reaction characteristics as also shown below:

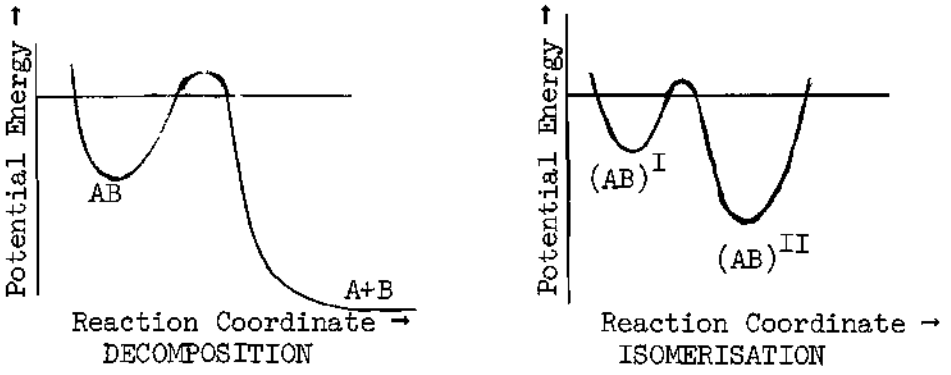

As a first step, these reactions at low temperatures and not at very low pressures, will be studied theoretically in the gas phase for non-polar and non-ionic molecules.

A. Bimolecular Gas Phase Reactions

Bimolecular (non-polar, non-ionic molecules) gas phase (not at very low pressures) reactions occurring at very low temperatures have very low activation energies for reaction. Reactions of this type can be assumed as having a relatively loose activated complex structure, in other words, the structure of the activated complex is very close to that of the reactants.

Ree, Ree, Eyring, and Fueno[60] calculated specific rates of radical association and ion-molecule reactions with the use of the absolute reaction-rate theory and compared the results with the observed values. From the results they concluded that the activated complexes of the fast reactions have loose structures such that the reactant molecules (radicals or ions) rotate freely with the restriction that they cannot move independently in the translational degrees of freedom.

A bimolecular reaction at very low temperatures will be considered to have both low activation energy and a relatively loose activated

complex structure. By strong interaction and configuration change within itself and by the loss of excess energy by some means, the activated complex comes to the configuration of the stable combined molecules.

The purpose of the present discussion is to derive an expression for the specific rate constant for bimolecular gas phase reactions with relatively loose activated complex structures. Two types of "loose activated complex"structures will be considered:

I. Loose activated complex with two internal rotations and one sluggish skeleton bending vibration.

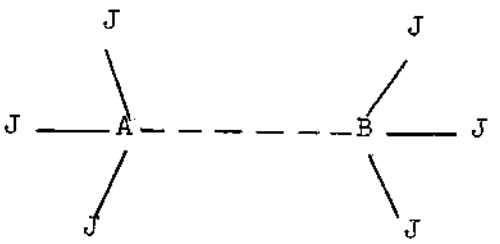

This type of complex structure will be used for reactions with low activation energies. A fast reaction with zero or very close to zero activation energy will have an activated complex structure with free rotation of the two groups. For reactions with little higher activation energy, the rotational motions of the two reactants will appear as two internal rotations around the axis joining A and B, one sluggish skeleton bending vibration, and three other bending vibrations. This type of activated complex structure will be considered to be the general activated complex structure for low activation energy reactions. The degree of looseness depends upon the amount of activation energy needed for reaction

and also the special features of that particular reaction. Now if one considers a more loose structure than in I above then one obtains the second type of extremely loose complex structure:

II. A loose activated complex with free rotation in the complex. This type of complex structure will be used for fast bimolecular reactions with almost zero activation energy. This can be used for some ion-molecule and free-radical reactions[60] also. The reaction cross-section for this case have already been developed[59].

$$\text{Reaction cross-section, } \sigma_{vmp} = \pi l_m^2 \hbar^2/2\mu E_p \qquad (1)$$

where l_m is the maximum value of l, the orbital angular momentum quantum number; E_p is the initial translational energy of the reactants in the Center-of-mass system and the other symbols have their usual meaning.

Reaction Cross-section for Complex I

Chemical-reaction cross-section will be calculated using a "Statistical-dynamical model" developed by Marcus[59] utilizing the activated-complex concept. This model assumes:

(a) Quasiequilibrium postulate between reacting pairs and activated complexes of the same energy and angular momentum; and a dynamical postulate:

(b) Adiabaticity of some degrees of freedom, where appropriate, and

(c) Only the initial energy along the reaction coordinate (the relative translational motion initially) and of any coupled adiabatic mode can be used to overcome the energy barrier. (The barrier arises

from any natural barrier, from the vibrational adiabatic effects, and from any centrifugal contribution). Thus, the theory has both statistical and dynamical features. This theory was developed for reaction for which activated complex configurations can be defined and for reactions with or without steric and activation barriers.

Terminology and Notations[59]

The following terminology and notations are used below for coordinates in the center-of-mass system.

Reactants: (a) three translations - one radial and two orbital, (b) adiabatic vibrations or rotations, (c) all others, henceforth called active modes.

Activated complex: (a) reaction coordinate q^r, (b) adiabatic vibrations (or rotations) coupled only to q^r throughout the motion, (c) all others, henceforth called active. Adiabatic modes are those which retain their quantum number (or classical action) on formation of activated complex from the reactants. A locally adiabatic approximation is used below for all coordinates other than q^r. The activated complex is defined as that q^r (denoted by q^{r+}) for which $\epsilon_{N^+}(q^r)$, the energy of the rotation vibration coordinates including potential energy of the q^r motion, has a maximum as a function of q^r.

The following notations will be used below for coordinates in the center-of-mass system.

Notation

q^r	Reaction coordinate
q^{r+}	Value of q^r at the activated complex
	It may vary with the quantum state N^+

p	Initial momentum of reactants in the center-of-mass system
k	Corresponding wavenumber ($= p/\hbar$)
μ	Reduced mass of the two reactants
E_p	Initial translational energy of reactants in the center-of-mass system ($= p^2/2\mu$)
N	Initial quantum state of pairs of reactants (exclusive of orbital angular momentum l and of its component), N denotes a pair of numbers v, n
v, E_v	Initial quantum state and energy of adiabatic degrees of freedom of pair of reactants, if any
n, E_n	Initial quantum state and energy of active degrees of freedom of pair of reactants
σ_{Np}	Reaction cross section for systems in an initial state N
σ_{vnp}	Reaction cross section for systems in an initial state v, n
γ	A summation operator involving summation over all geometric and optical isomeric reaction paths from reactants to activated complexes for the given process
V_o	Potential energy of most stable configuration of activated complex minus that for reactants
N^+	Quantum number of activated complex in a given vibration-rotation state N^+
K	Boltzmann's constant
n^+	Quantum number of active modes of the activated complex
$\epsilon_N{}^+$	Minimum energy needed for classical mechanical passage through the coordinate hypersurface, $q^r = q^{r+}$, in state N^+
$E_n{}^+$	Contribution of active modes to $\epsilon_N{}^+$
$\epsilon_v{}^+$	Contribution of adiabatic modes and of potential energy of q^r motion to $\epsilon_N{}^+$
$\bar{\epsilon}_v{}^+$	Average of $\epsilon_v{}^+$ for the given E
$E_v{}^+$	For Cartesian q^r energy of adiabatic modes in the activated complex ($E_v{}^+ + V_o = \epsilon_v{}^+$ for this Cartesian approximation)

E — Total energy in the center-of-mass system ($= E_v + E_n + E_p = E_n^+ + \epsilon_v^+ +$ kinetic energy of q^r motion)

V_c — Centrifugal potential

V_e — $\bar{\epsilon}_v^+ - E_v$

j — Initial rotational angular momentum quantum number. {If the two reactants have individual j's, j_1 and j_2, then j lies in the interval $(|j_1 - j_2|, \ldots, j_1 + j_2)$}

w_{lvnp}^J — Reaction probability of reacting pair with total angular momentum J, initial orbital angular momentum l, and in state specified by v, n, and p

w_{lvnp} — Reaction probability of pair specified by l, v, n, and p

$\omega(E_n)$, $\omega^+(\epsilon_{N^+})$ — Number of states n and n^+ per unit energy (i.e., at fixed v) when the energy of the active modes is E_n and when the activated complex is in the state N^+, respectively

$\gamma S(E-E_n)$ — $(k^2/\pi)\sigma_{vnp}$ (outside of threshold)

$\gamma S(E-E_j-E_j^+)$ — $(k^2/\pi)\sigma_{vjp}$ (at threshold)

$Q(s)$ — Partition function of active modes of reactant pair when $s = 1/KT$, $\sum_n \exp(-sE_n)$

A, A^+ — Constants in classical expressions for $Q(s)$ and $Q^+(s)$

A_{rot}, A_{rot}^+ — Rotational factors in A and A^+

$N_{vib}^+(x)$ — Number of vibrational states of the active modes of the activated complex when their energy does not exceed x

I, I^+, σ', σ'^+ — Moments of inertia and symmetry numbers for a molecule and for a activated complex

κ — Transmission coefficient for the given E and N^+, or given E, v, and n^+

$Q_A^{int.}$ — The molecular partition function for the internal states of the molecule A as defined by the sum over internal energy states ϵ_{ai}, $Q_A^{int.} = \sum \exp\left(\frac{\epsilon ai}{KT}\right)$

$Q_A^{rot.}$	The molecular partition function for the rotational states of the molecule A
E_{j_A}	Rotational energy for molecule A
j_A	Rotational quantum number for molecule A
j, E_j	Initial rotational quantum state and rotational energy of pair of reactants
E_j^+	Rotational energy of the activated complex
ν	Vibrational frequency of the reactants
ν^+	Vibrational frequency of the activated complex
ν'	Skeleton bending vibrational frequency for the activated complex
E_{act}	Activation energy

Based on the quasiequilibrium hypothesis equation (2) was derived[58] (see Appendix C) for a classical q^r motion:

$$\sum (k^2/\pi)\sigma_{Np} = \gamma \sum_{N^+} 1 \qquad (2)$$

where σ_{Np} is the reaction cross-section for a pair of reactants which are in an initial vibration rotation state N and which have an initial relative momentum p. $\sum_N$ and $\sum_{N^+}$ represent sums over all vibration-rotation state of the pair of reactants and of the activated complex, respectively, available to each pair or complex whose total energy is E(e.g., the second sum is over all N^+ for which $\epsilon_{N^+} \leq E$). γ, a second summation operator, denotes a summation over all optically and geometrically isomeric reaction paths leading to activated complexes for the process.

The adiabatic degrees of freedom (usually vibrational) remain

in approximately the same quantum state, ν, during formation of the activated complex. If n denotes the quantum number for the other rotation-vibration degrees of freedom of the reactants and if n^+ denotes those for the activated complex, N and N^+ denote the sets (v,n) and (v,n^+), respectively. In this case a sharper form of Eqn. (2) was obtained:

$$\sum(k^2/\pi)\sigma_{vnp} = \gamma\sum_{n+} 1, \tag{3}$$

$\sum_{n}$ and $\sum_{n^+}$ represent sums over all active vibration-rotation states of reactant pair and activated complex, respectively, available to each species whose total energy is E and whose adiabatic modes are in a specified state ν.

Dynamical Conditions for Reaction

The adiabatic modes and the q^r motion are strongly coupled, an increase in the energy of the one being compensated by a loss in the other. Their initial energy is $E_p + E_v$, since at large separation distances the q^r motion is the relative translational motion. At $q^r = q^{r+}$, the energy residing in the adiabatic modes, in the natural barrier, and in the centrifugal barrier is $\bar{\epsilon}_v^+ + V_c$. Consequently, for reaction to occur it is assumed $E_p + E_v \geq \bar{\epsilon}_v^+ + V_c$, which can be rewritten as $E_p \geq V$, where $V = V_c + V_e$ and $V_e = \bar{\epsilon}_v^+ - E_v$. A statistical assumption is made that the contribution of each reaction path to a reaction probability w^J_{lvnp} is a function only of the "excess", $E_p - V_e - V_c$, for that Jlvnp and path. Since $(k^2/\pi)\sigma_{vnp}$ equals a weighted sum over l of w^J's the following results are obtained: Outside of threshold, where V_c depends only on l, the contribution of each path to $(k^2/\pi)\sigma_{vnp}$ becomes a function

only of $E_p - V_e$. At threshold, where V_c was E_j^+, the contribution to $(k^2/\pi)\sigma_{vnp}$ becomes a function only of $E_p - V_e - E_j^+$.

Outside of the Threshold Region

The contribution of a reaction path to $(k^2/\pi)\sigma_{vnp}$ can be written as a function of $E - E_n$ for a given v, since $E_p - V_e$ equals $E - E_n - \bar{\epsilon}_v^+$. This function, denoted by $S(E - E_n)$, vanishes when $E - E_n$ becomes less than $\bar{\epsilon}_v^+$. Summing over all reaction paths, one obtains,

$$(\frac{k^2}{\pi}\sigma_{vnp}) = \gamma S(E - E_n) \tag{4}$$

Let $\omega(E_n)$ and $\omega^+(\epsilon_{N^+})$ denote the number of active modes' states per unit energy for reactants in state N and for activated complexes in the state N^+, respectively. These ω's refer to fixed v and do not include degeneracy of the adiabatic modes. $\omega^+(\epsilon_{N^+})$ is zero unless ϵ_{N^+} exceeds ϵ_v^+. Equation (3) now becomes

$$\int_{E_n = 0}^{E} S(E - E_n)\omega(E_n)dE_n = \int_{\epsilon_{N^+} = 0}^{E} \omega^+(\epsilon_{N^+})d\epsilon_{N^+} = \sum_{n^+} 1 \quad (\epsilon_{N^+} \leq E), \tag{5}$$

where the ϵ_{N^+} integral is performed at fixed v. The ω and ω^+ are sums of δ functions if the active modes are treated quantum mechanically. Otherwise, they are continuous.

Equation (5) is an integral equation for $S(E - E_n)$ and may be solved using Laplace transforms (6):

$$\bar{S}(s) = \int_0^\infty S(x) \exp(-sx)\, dx \tag{6a}$$

$$Q(s) = \int_o^\infty \omega(x) \exp(-sx)\, dx \tag{6b}$$

$$Q^+(s) = \int_o^\infty \omega^+(\epsilon_N^+) \exp(-s\epsilon_N^+)\, d\epsilon_N^+ = \sum \exp(-s\epsilon_N^+), \tag{6c}$$

Where the integration in Q^+ is performed at fixed v and where the summation is over all quantum states n^+, the v in N^+ being held fixed.

Multiplication of (5) by exp(-sE), integration of E from 0 to ∞, use of the convolution theorem of Laplace transforms and of the fact that the transform of the right side of (5) is $Q^+(s)/s$, yields

$$Q(s)\bar{S}(s) = Q^+(s)/s \tag{7}$$

Inversion yields S(y). It can be seen from (4) that y is to be set equal to $E - E_n$ to find the contribution of the path to σ_{vnp} for the given v, n, and p. So, one obtains the reaction cross-section for systems in an initial state v, n:

$$\sigma_{vnp} = \frac{\pi}{k^2} \frac{\gamma}{2\pi i} \int_{c - i\infty}^{c + i\infty} \frac{Q^+(s)}{sQ(s)} \exp\{s(E - E_n)\}ds \tag{8}$$

for $E - E_n \geq \epsilon_v^+$; σ_{vnp} is zero otherwise. In equation (8), c is the usual positive constant, chosen so that the poles of the integrand lie to the left of s = c in the complex plane.

Here $s = \frac{1}{KT}$, $Q^+(s)$ = A "partition function" (rotations, vibrations only) of an activated complex having a fixed v, $\sum_{n^+} \exp(-s\epsilon_N^+)$. $Q(s)$ =

Partition function (rotations, vibrations only) for active modes of reactant pair; $\sum_n \exp(-sE_n)$.

Now, we have to derive an expression of reaction cross-section from the general equation (8) for the low temperature model of exothermic bimolecular reaction. In this model, the activated complex had a loose structure with two internal rotation and one sluggish skeleton bending vibration.

Let us assume that the rotation-vibration interaction is negligible and dependence of q^{r+} on N^+ is negligible. We shall use the following expressions for partition functions: Partition function (rotations and vibrations only) $Q = Q_{rot}^3 \; Q_{vib}^{3N-6}$

$$Q_{rot}^3 = \frac{8\pi^2 (I_1 I_2 I_3)^{\frac{1}{2}} (2\pi KT)^{\frac{3}{2}}}{h^3 \sigma'} = \frac{(A_1 A_2 A_3)_{rot}}{s^{\frac{3}{2}}}$$

$$Q_{vib} = \frac{e^{-U/2}}{1-e^{-U}}, \text{ where } U = \frac{h\nu}{KT}.$$

Unless the vibrational frequency ν is very small, at very low temperature we will use $Q_{vib} \approx e^{-U/2}$. Since the vibrational frequency ν' in the sluggish skeleton bending vibration will be small, we approximate its partition function as $Q^+_{skel.\ bend.} = \frac{KT}{h\nu'}$.

Considering the above discussions and also the internal rotation in the activated complex, we get,

$$Q(s) = \frac{A_{rot}}{s^3} \exp\left(\frac{\sum \frac{U}{2}}{2(3N-6)}\right) = \frac{A_{rot}}{s^3} \exp(-sE_v)$$

$$Q^+(s) = \frac{A^+_{rot}}{s^2} \quad \frac{1}{sh\nu'} \exp\left(-\sum_{n^+} \frac{U}{2}\right) \exp\ (-sE_v)$$

So,

$$\frac{Q^+(s)}{Q(s)} = \frac{A^+_{rot}}{A_{rot}\ h\nu'} \exp\left(-\sum_{n^+} \frac{U}{2}\right) \tag{9}$$

Substituting this expression into equation (8), we get for reaction cross-section:

$$\sigma_{vnp} = \frac{\pi}{k^2} \frac{\gamma}{2\pi i} \int_{c\ -\ i\infty}^{c\ +\ i\infty} \frac{A^+_{rot}}{A_{rot}\ h\nu' s} \exp\ \{s(E - E_n - \sum_{n^+} \frac{h\nu^+}{2}]ds$$

or, $$\sigma_{vnp} = \frac{\pi}{h\nu' k^2} \frac{\gamma A^+_{rot}}{2\pi i A_{rot}} \int_{c\ -\ i\infty}^{c\ +\ i\infty} \frac{\exp\{s(E - E_n - \sum_{n^+} \frac{h\nu^+}{2}\}ds}{s}$$

or, $$\sigma_{vnp} = \frac{\pi\gamma A^+_{rot}}{h\nu' k^2 A_{rot} 2\pi i}\ 2\pi i\ \frac{\{E - E_n - \sum_{n^+} \frac{h\nu^+}{2}\}^o}{0!} \quad (\text{for } E - E_n \geq \bar{\epsilon}^+_v;$$

otherwise $\sigma_{vnp} = 0.$)

or, $$\sigma_{vnp} = \frac{\pi\gamma A^+_{rot}}{h\nu' k^2 A_{rot}}$$

or, $$\sigma_{vnp} = \frac{\pi\hbar^2 A^+_{rot}\gamma}{2\mu A_{rot.}(h\nu')E_p} \tag{10}$$

This expression for reaction cross-section will be used for general bimolecular reactions at cryogenic temperatures.

In our model for the bimolecular reactions, we considered the activated complex structure to be loose but not as loose as free rotation of the reactant groups. In the later case the steric factor should be close to one whereas in the other case the steric factor should have some moderate value depending upon the looseness of the activated complex structure. Now, comparing the reaction cross-section expressions (equation (1) and equation (10)) for these two cases, we find that they differ by the factor

$$\frac{A^{+}_{rot}}{A_{rot}(h\nu')l^{2}_{m}}$$

in equation (10) which depends upon the looseness of the activated complex structure. So, the idea in the low temperature reaction model is reflected in its chemical reaction cross-section expression.

Reaction Rate Constant for Bimolecular Reactions at Cryogenic Temperature

The general expression for specific rate constant k_R^{el}, with the assumption of thermal equilibrium for the translational degrees of freedom and for the internal degrees of freedom of the reactant molecules, is given by;

$$k_R = \frac{(\frac{2}{KT})^{\frac{3}{2}} \gamma \sum_j \exp(-E_j/KT)}{(\pi\mu)^{\frac{1}{2}} Q_A^{int} Q_B^{int}} \int_{E_{act}}^{\infty} \sigma_{vnp} E_p \exp(\frac{-E_p}{KT}) dE_p \qquad (11)$$

Substituting, equation (10) for σ_{vnp} into equation (11), we get,

$$k_R = \frac{\left(\frac{2}{KT}\right)^{\frac{3}{2}} \gamma}{(\pi\mu)^{\frac{1}{2}} Q_A^{int} Q_A^{int}} \sum_j \exp(-Ej/KT) \int_{E_{act}}^{\infty} \frac{\pi\hbar^2 A_{rot}^{+} E_p \exp\left(\frac{-E_p}{KT}\right) dE_p}{2\mu A_{rot}(h\nu')E_p}$$

$$k_R = \frac{\left(\frac{2}{KT}\right)^{\frac{3}{2}} A_{rot}^{+} \gamma \pi\hbar^2 KT \exp\left(\frac{-E_{act}}{KT}\right)}{(\pi\mu)^{\frac{1}{2}} Q_A^{int} Q_B^{int} 2\mu A_{rot}(h\nu')} \sum_{j_A, j_B} \exp\left(\frac{-E_{j_A} - E_{j_B}}{KT}\right) \qquad (12)$$

where the activation energy consists of the natural barrier, the centrifugal barrier, and the contribution from the adiabatic coordinates. To take into consideration of the threshold region approximately (see Appendix E), the right hand side of equation (12) should be multiplied by $\frac{(I^+ + I)}{I^+ C_1}$ so that, finally, we get, (i) at threshold region,

$$k_R = \frac{A_{rot}^{+} (I^+ + I) \exp\left(\frac{-E_{act}}{KT}\right)}{(KT)^{\frac{1}{2}} C_1 (2\pi\mu)^{\frac{3}{2}} I^+ Q_A^{rot} Q_B^{rot} A_{rot}\nu'} \sum_{j_A, j_B} \exp\left(\frac{-E_{j_A} - E_{j_B}}{KT}\right) \qquad (13a)$$

(ii) outside threshold region,

$$k_R = \frac{A_{rot}^{+} \exp\left(\frac{-E_{act}}{KT}\right)}{(KT)^{\frac{1}{2}} (2\pi\mu)^{\frac{3}{2}} Q_A^{rot} Q_B^{rot} A_{rot}\nu'} \sum_{j_A, j_B} \exp\left(\frac{-E_{jA} - E_{jB}}{KT}\right) \qquad (13b)$$

The rate equation developed above for bimolecular reactions at low temperature can serve several purposes in different degrees:

(a) It shows how the different variables affect the rate of bimolecular low-temperature reactions in the gas phase.

(b) It gives a computable mathematical expression for the specific rate constant.

The main assumption in computing the activation energy using INDO or MINDO molecular orbital method was as follows: Since the activated complex is loose, its identity is not much different from the reactants; so the error involved in the calculation of their total energies will be in the same direction and almost of same order of magnitude; so when one calculates the activation energy by taking difference of their total energies, those errors in the calculation should tend to cancel each other. Also, the errors inherent in the INDO approximations increase with decreasing distances as the neglected electron populations become more important.

To compute the specific rate constant, we need to know molecular geometries, A^{+}_{rot}, rotational energy levels of the reactants, E_{act}, and ν'. If we compute the geometry and total energy of the activated complex and reactants by the MINDO/2 method for hydrocarbons as described by Dewar[56] and by the INDO method for other compounds, then we can estimate E_{act} and A^{+}_{rot}. In addition, ν' can be computed by MO methods from the energy involved in performing such motion[56,57] in the activated complex. The quantum mechanical energy of rotation of polyatomic molecules has not been expressed in closed form, but it has been tabulated for a large range of quantum numbers and moments of inertia[71].

For computation of the expressions (13a) and (13b) at low temperature, the higher rotational energy levels will not have much contribution so the computation of rotational energy levels will not be much involved.

The advantage of loose structure of the activated complex and low activation energy will decrease to a great extent the amount of MO calculation that is needed. The accuracy in the calculation of rate constant depends upon the correctness of the MO methods used in simultaneously calculating geometry and energy.

The reaction between two CF_3 radicals to give C_2F_6 has been studied by the INDO method by following the minimum energy path for the approach of two CF_3 free radicals, $2CF_3 \rightarrow C_2F_6$. Activated complex:

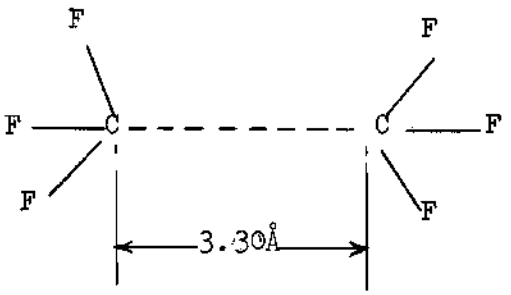

Value of activation energy (excluding centrifugal barrier) is found to be $E_{act} < 1$ kcal. It has also been found that the multiplicity of the (C_2F_6) complex changes from 3 to 1 at a C-C distance of 2.45 Å.

Assuming zero activation energy, the reaction was found experimentally to have a steric factor of 0.16[63].

This calculation shows that INDO method can be used in our scheme of calculation. So we can handle molecules with atoms from 1st row in the periodic table. The MINDO/2 method has already been shown to be satisfactory in geometry and energy calculations for hydrocarbons.

(c) It attempts to predict the chemical reactivity at low temperature and thereby the useful existence of a compound as a cryochemical reagent.

This point needs further discussion. In this case the first step is to postulate a bimolecular reaction, say $AJ_3 + AJ_3 \rightarrow$ Activated complex $\rightarrow$ Products.

The next step is to compute the activation energy of this reaction by the MO methods. If the activation energy is low, then this computation should not be much involved due to the loose structure of the activated complex and one should go to the next step. If the activation energy is not low then this computation will be much more involved but one can conclude its cryogenic existence. If the activation energy is low, the next step is to compute the specific rate constant using the MO methods and the equation for k_R developed earlier (equation 13). This will give an idea of chemical reactivity in the gas phase.

A roughly quantitative comparison of solution and gas phase reaction rates had been made by Benson[62] assuming an ideal solution and using Raoults' law. In this comparison, he assumes the reaction is such that the reactants form a loosely bound activated complex and also the free volume of the liquid are about one per cent of their molar volumes. Using these assumption, he compares the specific rate coefficient in the solution k(s) with the specific rate constant in the gas phase k(g) by the following equation:

$$\frac{k(s)}{k(g)} = \frac{n\ 10^{2n-2}}{e^{n-1}} \qquad (14)$$

where n is the molecularity of the reaction. The values of k(s)/k(g) predicted for unimolecular, bimolecular and trimolecular reactions (n = 1,2,3) are 1,86, and 4050 respectively. The prediction that a

unimolecular reaction would proceed at about the same rate in both cases has been supported experimentally for the few reactions that have been studied in both phases. The predicted effect of the presence of a solvent on the rate of a bimolecular reaction agrees qualitatively with the predicted increase. However, experimental results for bimolecular reactions, which are thought to occur by the same mechanism in both phases, are too sparse to provide a test of these predictions.

From the estimated specific rate constant in the gas phase and its comparison with the liquid phase reaction as discussed above, one can obtain a rough quantitative idea about the reaction rate in the liquid phase. How well this rough quantitative idea will describe the reaction of a pure liquid at low temperature is not known, however, k(s) multiplied by the concentration factors in the liquid should give some idea about the rate of reaction in the liquid phase. If the rate is extremely low at its melting point then one can expect its useful cryogenic stability and existence.

If the rate is relatively fast in the liquid then its useful cryogenic stability is in question. In this case if the reaction is highly exothermic and the rate of heat transfer to the cold wall is low then the temperature will increase and there is a possibility of an explosive reaction. Reaction rates in the solid phase or at a solid-liquid interface will be much slower than in the liquid phase.

Reaction of Borane with Borane Using the INDO Method

To study the features of the reaction between highly reactive compounds from a theoretical perspective, the reaction of two borane molecules to form diborane has been studied using the INDO molecular

orbital method. The main purpose was to determine a portion of the minimum energy path (excluding centrifugal effects) for two approaching borane molecules to form diborane. From such a study one can also obtain the type of activated complex structure and some idea about the activation energy. Since the INDO method[55] is more or less good for predicting the geometry of molecules and also the difference in energy calculated by INDO of two very similar molecules can be considered to be good, this method was considered to be satisfactory for the present purpose.

Using the INDO method the minimum energy path for the approach of two borane molecules to each other was found by approaching the two molecules in several possible ways with simultaneous possible changes in configuration. These calculations have been described in Appendix D in more detail. The minimum adiabatic energy path for the process was as follows:

(1) Approach of two borane molecules as shown below up to a B-B distance of 3.40 Å.

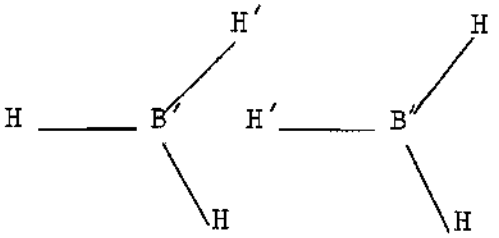

(2) Then rotating $B'H_3$ in a clockwise direction with simultaneous twisting of $B'H'$ and $B''H'$ away from the plane in opposite directions as the two borane molecules approach each other.

The structure of the complex in this minimum energy path having

maximum energy is considered to be the activated complex structure (excluding centrifugal effects) and it is as shown below.

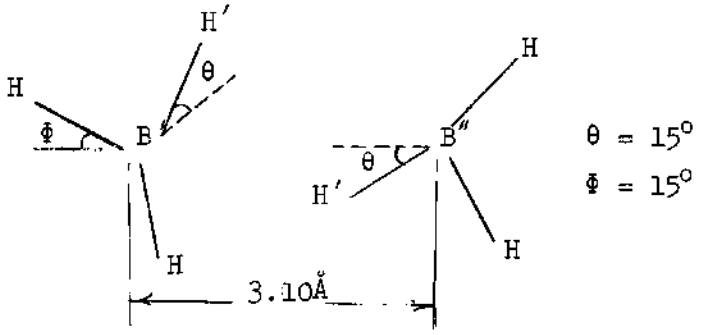

No changes in B-H bond lengths were found. Diborane has bridge structure, with the bridge atoms above or below the plane of other atoms (distances in Å).

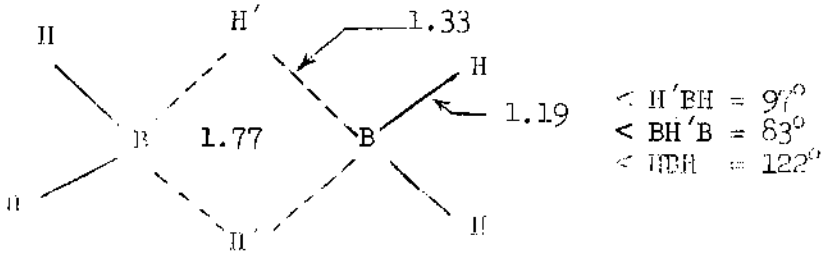

Structure of borane is as follows:

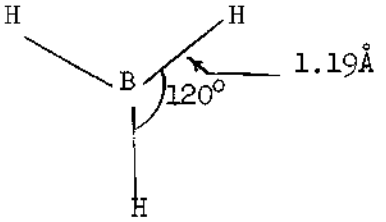

Considering the structures of borane, the activated complex, and diborane, it is clear that the activated complex is more similar to the two borane molecules and also the activated complex structure is loose but not too loose to perform free rotation.

This finding supports the postulate that for fast bimolecular reactions the activated complex structure will be loose.

The activation energy (excluding centrifugal barrier) for this reaction is obtained by subtracting the energy of two borane molecules from the energy of the activated complex, and it is found to be equal to 1.849 kcal/mole. This shows that for a small change in configuration, there is a small change in energy. This supports the idea that low activation energy reactions will have loose activated complex structure.

Considering the high chemical reactivity of borane, the activation energy looks reasonable, however, one can question its accuracy.

B. Unimolecular Exothermic Decomposition and Isomerization Gas-Phase Reactions at Cryogenic Temperature

(1) Decomposition: Conditions for a low temperature model.

(a) Structure of the molecule as well as of the activated complex are loose at the breaking bond; i.e. A and B are connected by a weak bond.

(b) Molecule and the activated complex will have some low frequency bending vibrations and internal rotations; one has to consider them in computing the partition functions. Specific rate constant for decomposition at the high pressure limit $k_{d\infty}$ using Marcus'[68] quantum mechanical transition state formulation is given:

$$k_{d\infty} = \kappa \frac{KT}{h} \frac{Q^{+}_{rot}}{Q_{rot}} \frac{Q^{+}_{vib}}{Q_{vib}} e^{-E_a/RT}$$

where Q_{rot} = rotational partition function of the reactant; Q^{+}_{vib} = vibrational partition function of the activated complex; E_a = activation energy; κ = transmission coefficient.

Most of the vibrational modes will be adiabatic and they will cancel each other. So we have to compute E_a, structure of the molecule and the complex, and one or two bending vibrational frequencies by the MO method. Transmission coefficient $\kappa = 1$ is a very good assumption in this case.

In the low pressure limit, the specific rate constant will be given by,[69]

$$\frac{k_{d,o}}{n} \approx \frac{I^*}{Ie} \frac{Z}{\gamma(s)} \frac{(E_a)^{S-1}}{(KT)^{S-1}} \exp\frac{(-E_a)}{(KT)} \left\{1 + \frac{S-1}{\frac{(E_a)}{KT}} + \ldots + \frac{(S-1)!}{\left(\frac{E_a}{KT}\right)^{S-1}}\right\}$$

where S = number of specified oscillations to be determined or guessed; n = number of molecules per unit volume; Z = effective collision number per unit volume per unit time at unit concentration; E_a = activation energy.

(2) Exothermic Isomerization Reactions

The same equations for specific rate constants as were mentioned above can be used in this case. The activated complex will be more similar to the reactant and some of the vibrations will be adiabatic. For each reaction one has to carefully follow the path from the reactant to

the activated complex. The transmission coefficient may be a serious factor in this case. Since $\kappa = 1$ will give the upper limit of isomerization, one can still comment on the cryogenic stability.

To take into account the quantum mechanical tunneling, one should multiply the right hand side of specific rate constant equations by a tunneling correction factor κ'.

To find whether the tunneling factor is important or not, one should calculate the Boltzmann-de Broglie wave length

$$\lambda = 17.45/(MT)^{\frac{1}{2}} \text{ Å}$$

where M is molar mass and T is temperature in ^{O}K.

If λ is of comparable length to dimensions of the activated complex then the tunneling factor is important. If λ is too small then one can use $\kappa' = 1$, in other words, one can neglect tunnel effect.

Wigner[72] showed that for the passage of a particle of mass m, the first approximation to the tunnel correction (assumed small) can be written as $\kappa' = 1 + h^2A/96\pi^2mK^2T^2$ where A is curvature of the energy surface.

It is clear from this expression that at low temperatures and for system with low molecular weight, the tunneling effect becomes an important factor. For example, using unsymmetrical Eckert potential barrier for certain conditions and temperature T_1 the tunneling correction factor is 1.12 whereas it becomes 23.3 under the same conditions but temperature $T = T_1/8$[73]. Lower molecular weight systems will also have similar effects. In these cases where the tunnel effect is important one can approximate it for q^r motion by using R. P. Bell's[70] tunnel

effect correction factor of a parabolic energy barrier as follows: For $\alpha > \beta$, the tunnel correction factor

$$\kappa' = \frac{\alpha \exp(\alpha-\beta)}{\alpha-\beta} \{1 + 0(\exp(-\beta)\},$$

where $\alpha = \frac{E_{act}}{KT}$ and $\beta = 2\pi^2 a (2m E_{act})^{\frac{1}{2}}/h$, 2a = width of the barrier. This equation is applicable for large degrees of tunneling. For $\alpha < \beta$ the tunnel correction factor κ' is approximated by,

$$\kappa' = \tfrac{1}{2} U/\mathrm{Sin}\tfrac{1}{2}U, \quad \text{where } U = 2\pi\alpha/\beta$$

Johnston[74] applied this equation to some known reactions and found it to overestimate the factor at low temperatures. He suggested a two dimensional solution for the problem.

For reactions with low activation energy, the width of the reaction barrier will be large due to comparable contributions from centrifugal effect. Due to this effect and also the fact that there is not enough potential barrier to be transmitted through, the tunnel effect should be low. So, if the molecular weight of the system is not too low, one can neglect the tunnel correction. However, when the tunnel effect is important one should use Bell's equation[70] for the purpose.

CHAPTER III

CONCLUSIONS AND RECOMMENDATIONS

The work described in the preceeding chapters has led to the following conclusions:

(1) An overall sequence or method has been proposed to understand the possibility of cryogenic synthesis of some unknown compounds.

(2) Theoretical models have been proposed to study the chemical reactivity and stability of a compound at cryogenic temperatures.

(3) Assuming low activation energy and a loose activated complex structure, a formulation of the specific rate constant for bimolecular gas phase reactions at cryogenic temperatures has been developed using Marcus' statistical-dynamical model for total chemical reaction cross-sections.

(4) The computation method of reaction characteristics for reactions at cryogenic temperatures using recent molecular orbital methods has been briefly described.

(5) Part of the minimum adiabatic energy path, activated complex structure, and approximate activation energy for the reactions $CF_3 + CF_3 \rightarrow C_2F_6$ and $BH_3 + BH_3 \rightarrow B_2H_6$ have been computed using the INDO molecular orbital method. The results look reasonable and support the postulate of a loose activated complex structure for gas phase reactions at cryogenic temperatures.

(6) The computation of reaction feacutres depends upon how well

developed the molecular orbital method is and also the assumptions involved in the method. Although for low temperature reactions the present MO methods can be argued to be satisfactory, it would nonetheless be better if a better method for calculating reaction features were available.

Several extensions of the present work may be recommended:

(1) Specific rate constants for several known gas phase reactions at cryogenic temperatures particularly bimolecular reactions should be computed in the way described in the present work and the chemical reactivity and stability features should be compared.

(2) Experimental reaction kinetics study of some such reactions should be made to give more insight into low temperature reaction kinetics and also to find out the agreement with the computed results.

(3) Since the computation scheme depends upon the molecular orbital methods, one should use the best method suited for the purpose assuming that there will be more development of these methods.

APPENDICES

APPENDIX A

BRIEF DESCRIPTION OF INDO AND MINDO MOLECULAR ORBITAL METHODS

The INDO method[55] deals with approximate methods for calculating a single determinant molecular wave function for all valence electrons of a molecule. The molecular wave function is considered as a determinantal product of one-electron molecular orbitals ψ_i which are taken as linear combinations of an atomic orbital (LCAO) basis set, made up of atomic functions from the valence shell of each atom in the molecule (valence basis set). Finding the set of linear coefficients which minimize the total energy of the system under consideration is accomplished by the LCAO self-consistent-field (SCF) method[64], with approximations invoked in the calculation of the matrix elements of $F_{\mu\nu}$ of the Hartree-Fock Hamiltonian operator.

In order to obtain results which are invariant under local rotation and hybridization of the atomic-orbital basis set, it can be shown that only certain types of approximate schemes are permissible. Two of these are: (1) the complete neglect of differential overlap (CNDO) in which a product of two different atomic orbitals $\phi_\mu(1)\ \phi_\nu(1)$ associated with Electron 1 is always neglected in electron-interaction integrals and (2) the neglect of diatomic differential overlap (NDDO) in which this product is only neglected if $\phi_\mu(1)$ and $\phi_\nu(1)$ are on separate centers.

One of the major limitations of the CNDO method[57] is the exclusion of one-center exchange integrals. The more complex NDDO method has

the disadvantage of requiring the calculation of a much larger number of two-center integrals. There is, however, an intermediate possibility in which one-center products $\phi_\mu(1)\,\phi_\nu(1)$ involving different atomic orbitals ϕ_μ and ϕ_ν are retained only in one-center integrals. Such a procedure still retains the necessary invariance properties and is intermediate in complexity between CNDO and NDDO. It is referred to as the method of "Intermediate Neglect of Differential Overlap" (INDO). In this method, the evaluation of the elements of the Hartree-Fock Hamiltonian F matrices is simplified by a set of five approximations. The approximations in detail are:

Approximation 1: The overlap integrals $S_{\mu\nu}$ are neglected unless $\mu = \nu$. This reduces the LCAO-SCF equations to the form $F^\alpha C^\alpha = C^\alpha E^\alpha$, $F^\beta C^\beta = C^\beta E^\beta$ where C^α is the matrix of linear expansion coefficients for α electrons, and E^α and E^β are matrices for orbital energies.

Approximation 2: The two-, three- and four-center integrals of the type $(\mu\lambda/\nu\sigma)$ are set equal to zero unless $\mu = \lambda$ and $\nu = \sigma$. Those which remain are further simplified by the approximation $(\mu\mu/\nu\nu) = \gamma_{AB}$ (μ on A, ν on B), where γ_{AB} is approximated as the coulomb integral $(s_A s_A/s_B s_B)$ involving valence shell s-type orbitals of the atoms A and B with which μ and ν are respectively associated.

Approximation 3: The diagonal core-matrix elements are calculated by separating the interactions of ϕ_μ (centered on atom A) wuth the core of A and with the other atomic cores,

$$H_{\mu\mu}^{core} = U_{\mu\mu} - \sum_{B(\neq A)} Z_B \gamma_{AB}.$$

The corresponding one-center core integrals $U_{\mu\lambda}$ ($\mu \neq \lambda$, both centered on atom A) will vanish if a pure s and p basis set is used, but would be non-zero for hybrids.

Approximation 4: The two-center core-matrix elements $H_{\mu\nu}^{core}$ are approximated by

$H_{\mu\nu}^{core} = 1/2\ (\beta_A^o + \beta_B^o)\ S_{\mu\nu}$ (μ on A, ν on B), where β_A^o and β_B^o are empirical parameters selected for the CNDO method[57].

Approximation 5: The one-center electron-interaction integrals are specified as follows in terms of the Slater-Condon F^k and G^k parameters, and assuming 2s and 2p orbitals to have the same radial parts:

$(ss/ss) = (ss/pp) = F^o = \gamma_{AA}$

$(sp/sp) = 1/3\ G^1$

$(pp'/pp') = 3/25\ F^2$

$(pp/pp) = F^o + 4/25\ F^2$

$(pp/p'p') = F^o - 2/25\ F^2$

and similar expressions for (ss/zz), etc. The integral F^o (or γ_{AA}) are evaluated from Slater orbitals, but semi-empirical values are used for G^1 and F^2 which correspond to those given by Slater[65] to give best fits with atomic experimental data. The core integrals $U_{\mu\mu}$ are also found semi-empirically by subtracting electron interaction terms from the mean of the ionization potential I and electron affinity A of appropriate atomic states. This INDO method have been tested for calculating molecular geometries and other parameters, and it has been found to be

quite satisfactory for this purpose and in particular for calculating bond angles[55].

Description of MINDO Method

The MINDO (modified INDO) method[40,56] differs from the INDO method in several respects. In the first place, the INDO method was meant for finding a simple procedure that would reproduce the result that would be given by exact Hartree-Fock calculations, were these possible. The parameters in this treatment were chosen accordingly, and the heats of formation given by them could not therefore be in even approximate agreement with experiment. On the other hand, the MINDO method has been concerned primarily with calculating heats of formation and other ground state properties. The parameters in this treatment were therefore chosen to fit the observed properties of suitable reference molecules, rather than the results of a priori calculations. Second, the one-center integrals used in the molecular calculations are derived from an analysis of the atomic spectra of the first-row atoms. As in the INDO method, the one-center core-electron attraction integrals are denoted U_{ss} and U_{pp}, and the one-center electron repulsion integrals are written in terms of the Slater-Condon F^k and G^k parameters. The values for G^1 and F^2 used in the INDO method were used, and U_{ss}, U_{pp}, and F^0 were evaluated for each atom, having the ground-state configuration $s^n p^m$, by using the transition energies among the high-spin states of the configurations $s^n p^{m+1}$, $s^n p^m$, $s^n p^{m-1}$, and $s^{n-1} p^{m+1}$. Klopman's approximations: (ss,ss) = (ss,pp) = (pp,pp) = pp,p′p′) and (sp,sp) = (pp′,pp′) were not used in this method since these approximations do not lead to molecular energies which are invariant with respect

to a rotation of molecular axes in space in the INDO framework of approximations. Thirdly, the various two-center integrals in the MINDO method were estimated by a simple scheme analogous to that used in the Pariser-Parr treatment of π systems.

The core-core repulsion integrals have been set equal to the electron-electron repulsions. So, the total molecular energy can be written,

$$E = 1/2 \sum_u \sum_v P_{uv} (H_{uv} + F_{uv}) + \sum_{A<B} \sum C_A C_B \gamma_{AB}$$

or

$$E = \sum_i^{occ} \epsilon_i + 1/2 \Sigma \Sigma P_{uv} H_{uv} + \Sigma \Sigma C_A C_B \gamma_{AB},$$

where ϵ_i is the one-electron orbital energy for MO ψ_i, and the summation $\sum_i^{occ}$ runs over all doubly occupied MO's. The total bonding energy of a molecule can then be calculated from E by subtracting the sum of the isolated atom energies for the component atoms of the molecule. The heat of formation is then obtained by subtracting the sum of the ΔH_f values for the isolated atoms from the bonding energy.

Resonance Integrals in MINDO Method.

Since all resonance integrals between AO's of different atoms are considered explicitly in modern valence-electron MO methods (i.e., no distinction is made a priori between "bonded" and "nonbonded" interactions) the semiempirical expression for β_{uv}^c must reflect both the correct angular behavior and the appropropriate dependence on internuclear distance for each atom pair. The appropriate angular dependence, and the approximate distance dependence, is obtained by setting β_{uv}^c proportional to the

corresponding overlap integral, S_{uv}. It is also necessary to set β^c_{uv} proportional to a mean of the neutral-atom valence-state ionization potentials I^A_u and I^B_v of the AO's ϕ_u of atom A, and ϕ_v of atom B, if $\beta^c_{uv} = S_{uv}\ (I^A_u + I^B_v)\ f\ (R_{AB})$, where I_u is taken as the energy required to remove an electron from the singly occupied AO u, assuming that the remaining valence electrons of the neutral atom are evenly spread among the other valence-shell atomic orbitals, and that the spins of the valence electrons are randomly oriented with respect to the electron being removed. Here $f(R_{AB})$ is a function of the internuclear distance R_{AB} between A and B. For example, for hydrocarbons various two-parameter functions for C-C bonds were tried, retaining the simple approximation for H-H and C-H bonds; the most successful simple function was of the form $f(R_{AB}) = \beta^I_{cc} + (\beta^{II}_{cc}/R^2_{AB})$, where β^I_{cc} and β^{II}_{cc} are empirically determined parameters. Extensive trials showed that no advantage was gained by introducing the additional term into the expressions for H-H and C-H bonds; here $f(R_{AB})$ was set equal to constants β_{HH} and β_{CH}, respectively, these being found by fitting the heats of formation of H_2 and CH_4. For hydrocarbons, the β^I and β^{II} parameters and also the standard bond lengths and standard bond angles for different kinds of bonds - have been obtained by fitting to known heats of formation of various hydrocarbons. The heat of formation and ionization potential of any hydrocarbon molecule can be calculated by the MINDO/1 method if the geometry of the molecule with standard bond lengths and standard bond angles is supplied to the MINDO/1 program as input data. The MINDO/1 program can also be used for other types of compounds if the β^I and β^{II} parameters, and standard geometry for that type of compound are obtained by fitting to

the heats of formation of that type of compound. The MINDO/1 method has demonstrated superior accuracy in calculating heats of formation and ionization potentials of a wide variety of compounds, particularly hydrocarbons.

Dewar and Haselbach[56] have written a computer program for automatically optimizing the parameters in MO treatments. Using this, and using parametric functions for the core resonance integrals and core-core repulsions similar to those used in the PNDO approximation, they were able to develop a version (MINDO/2) of the MINDO method which gives good estimates of bond lengths, heats of formation, and force constants simultaneously for a wide variety of hydrocarbons, thus satisfying the minimum requirements for a procedure to be used convincingly for calculating potential surfaces.

The one-electron resonance integrals β^c_{ij} were represented by functions of the type, $\beta^c_{ij} = BS_{ij}\ (I_i + I_j)\ f_1\ (r_{ij})$ where $f(r_{ij})$ is a function of the internuclear distance r_{ij} and B is a parameter. The core repulsion between atoms m and n, i.e. CR_{mn} was represented by the expression $CR_{mn} = ER_{mn} + (Z_m Z_n \frac{e^2}{r_{mn}} - ER_{mn})\ f_2(r_{mn})$ where $f_2(r_{mn}) \underset{\to 1}{\to 0}$

as $r_{mn} \to \infty$

as $r_{mn} \to 0$

where the function f_2 contains a parameter α that determines the internuclear distance at which CR_{mn} begins to deviate from the electron-electron repulsion integral between neutral atoms, i.e., ER_{mn}.

After parametrization with respect to the properties of hydrocarbon molecules, the following values for the parameters were obtained:

$f_1 = 1$, $f_2 = \exp(-\alpha r_{mn})$; $B_{CC'} = 0.36862$; $B_{CH'} = 0.34104$; $B_{HH'} = 0.48328$; $\alpha_{CC'} = 1.6343 \text{Å}^{-1}$; $\alpha_{CH'} = 1.1843 \text{Å}^{-1}$; $\alpha_{HH'} = 0.6653 \text{Å}^{-1}$. So the MINDO/2 method can, at present, be used for hydrocarbons. Before it can be used for other types of molecules, it has to be parameterized with respect to those types of molecules. The MINDO/2 method has been used to calculate the potential surfaces[56] for the torsional isomerization of ethylene and cumulenes, for hydrogen abstraction reactions of methyl, and for the dimerization of ethylene. The results are encouraging as may be seen from Table A1. The method gives good estimates of first ionization potentials.

Table A1

Reaction	Activation Energy Calculated by MINDO/2 Method, kcal/mole	Experimental Activation Energy, kcal/mole
$H_3C^{\cdot} + H - CH_3 \rightarrow H_3C - H + {}^{\cdot}CH_3$	11.6	14.63 ± 0.3
$H_3C^{\cdot} + H - C_6H_5 \rightarrow H_3C - H + {}^{\cdot}C_6H_5$	10.8	9.3
Cumulenes; Rotation about the C = C Bond	54.1	65

APPENDIX B

IONIZATION EFFICIENCY CURVES

This appendix represents ionization efficiency curves in Figures 5-9 for the following: $I(BH_3)$ from the pyrolysis of BH_3CO; and $A(BH_3^+)$, $A(BH_2^+)$, $A(BH^+)$, and $A(B^+)$ from BH_3CO.

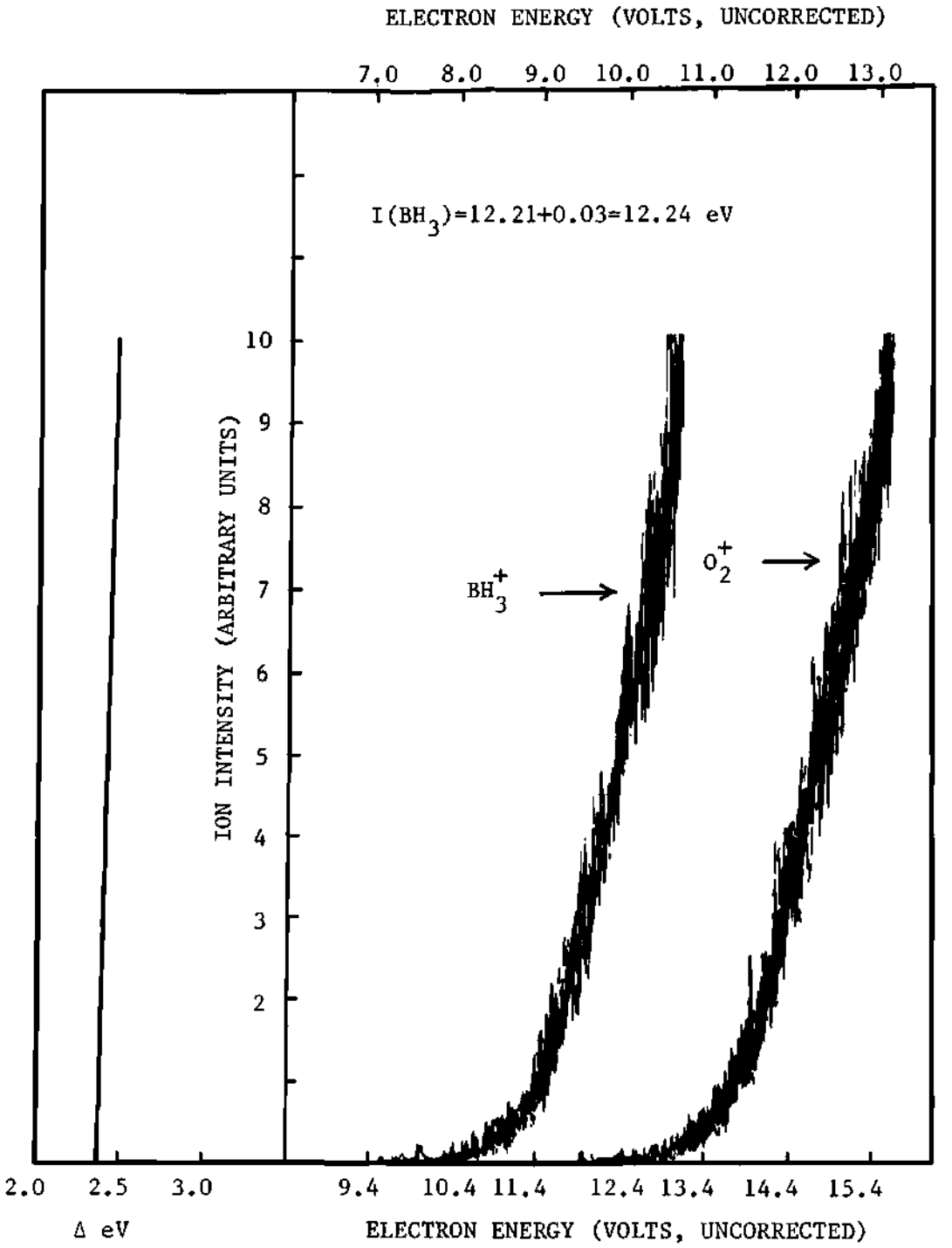

Figure 5. Ionization Efficiency Curve of BH_3 from the Pyrolysis of Borane Carbonyl.

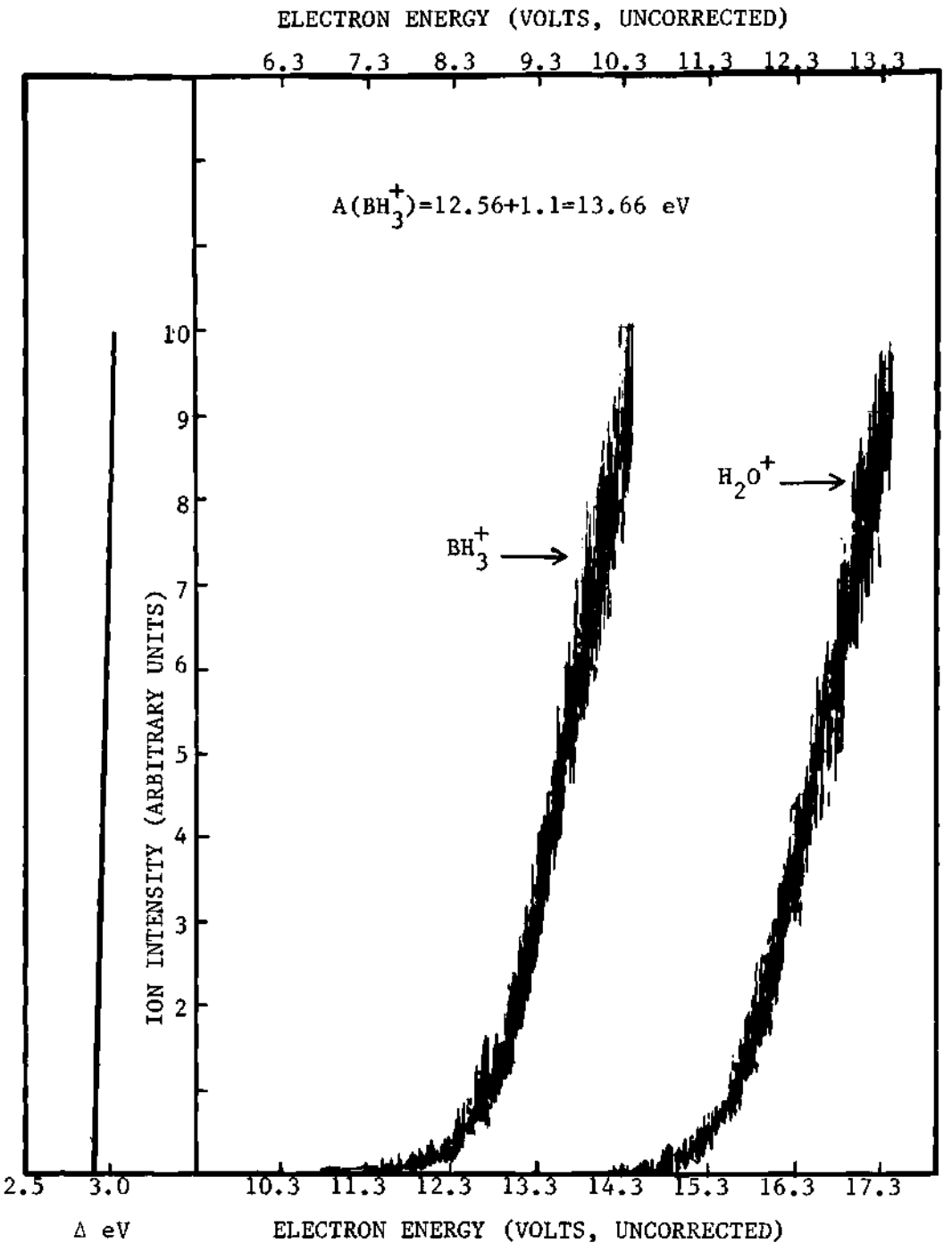

Figure 6. Ionization Efficiency Curve of $^{11}BH_3^+$ from BH_3CO.

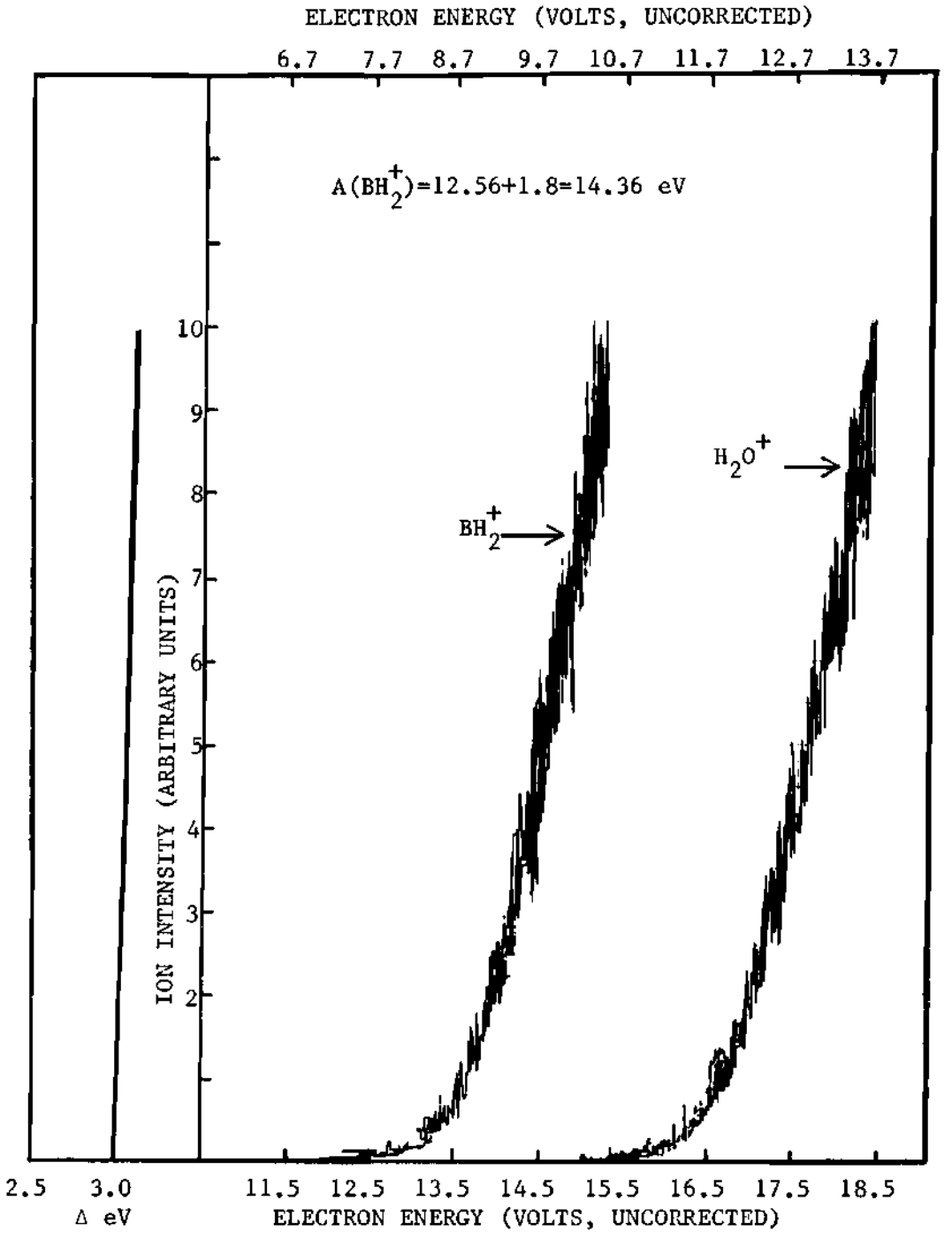

Figure 7. Ionization Efficiency Curve of $^{10}BH_2^+$ from BH_3CO.

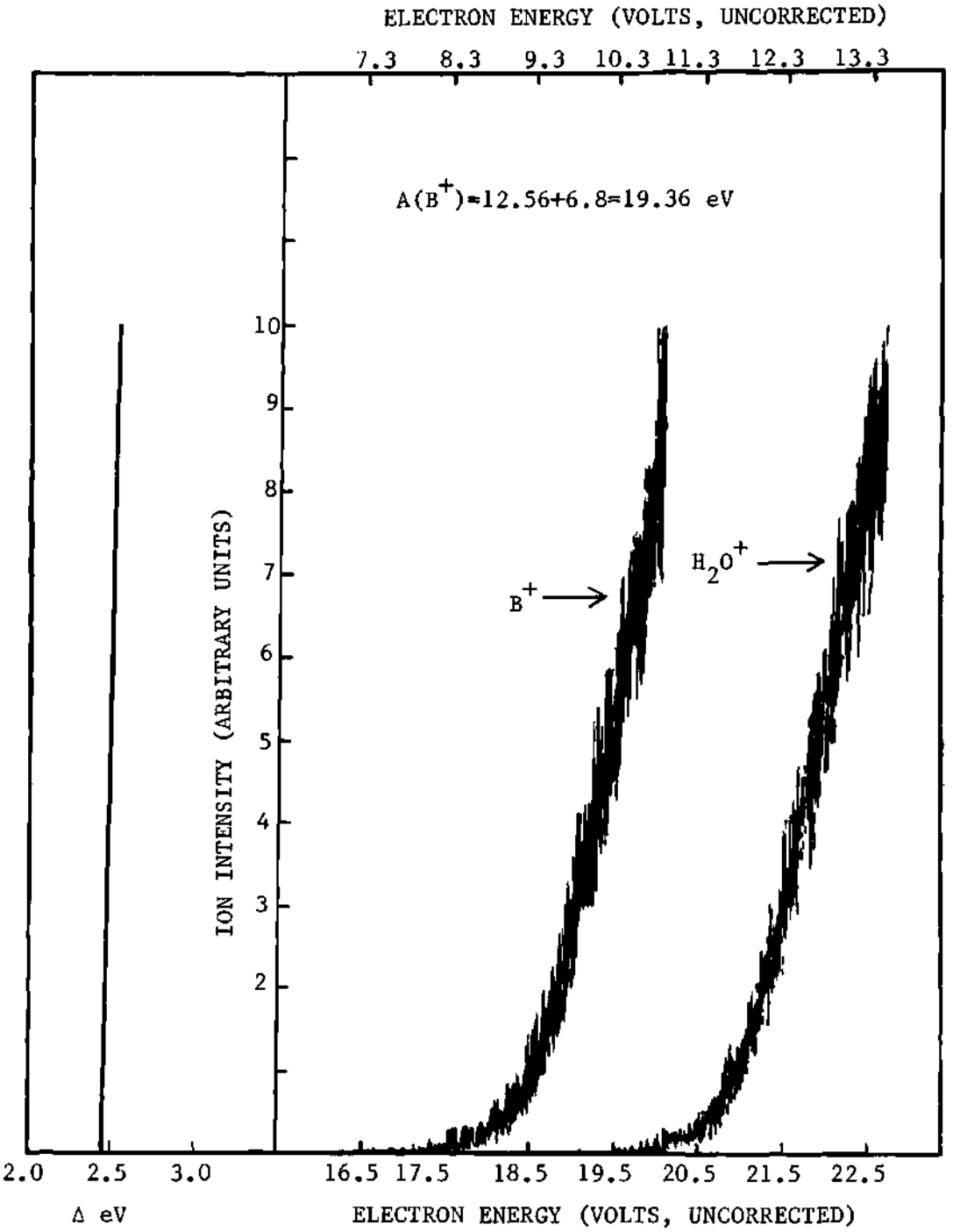

Figure 9. Ionization Efficiency Curve of $^{10}B^+$ from BH_3CO.

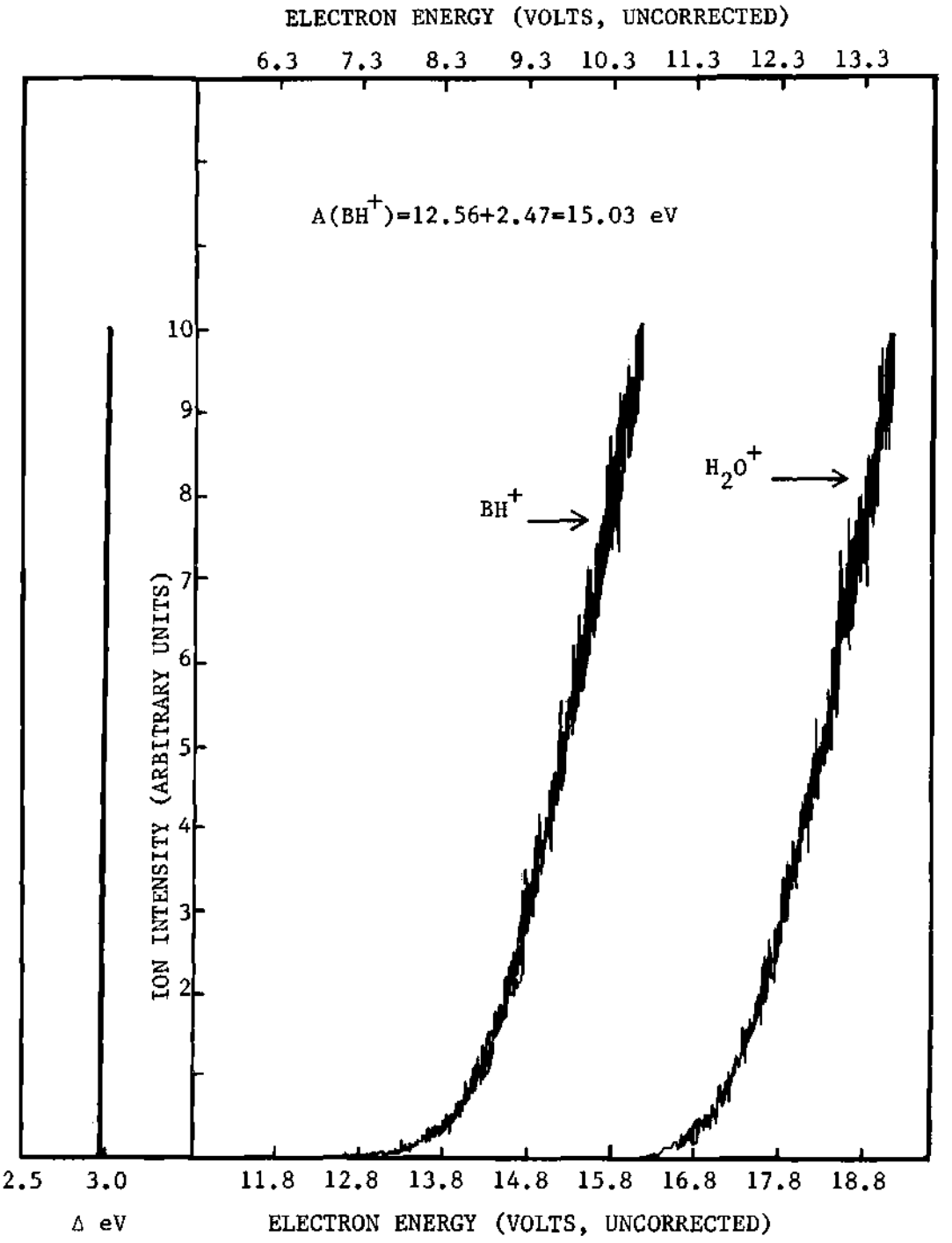

Figure 8. Ionization Efficiency Curve of BH^+ from BH_3CO.

APPENDIX C

MARCUS' QUASIEQUILIBRIUM THEORY FOR REACTION[58]

A quasiequilibrium hypothesis appears in a prominent way in the activated-complex theory of chemical reactions. This hypothesis is used to obtain equations relating sums over reaction cross-sections to properties of activated complexes.

Quasiequilibrium Hypothesis

During a collision the energy E, the total angular momentum quantum number J and its component along some axis M are conserved. In terms of the activated complex concept a quasiequilibrium hypothesis can be described as follows: when all quantum states of a reacting pair having a given J, M and a total energy within (E, E + dE) are made equally likely, all quantum states in the activated-complex region having this J, M and (E, E + dE) are also equally likely, each occurring with the same probability as those of the pair. An ensemble of reacting pairs is considered, uniformly distributed among all quantum states in the energy range E, E + dE. The total probability flux F of the products with the total energy lying in (E, E + dE) is given by:

$$F = \sum_{N} 4\pi p^3 dp \, \frac{\sigma_{Np}}{\mu h^3 \Pi} \tag{1}$$

where Π is the number of translational-rotational-vibrational quantum states of a relating pair in the range (E, E + dE) when the pair is in

a volume V. Other notations have been described in chapter II of part II of this thesis.

If q^r is the reaction coordinate and p_r is its conjugate momentum, the probability of the reacting pair being in the phase-space volume element $dq^r dp_r$ and in a rotation-vibration quantum state N^+ of the activated complex is $dq^r dp_r/h\Pi$ by the quasiequilibrium hypothesis. The net flow F through a q^r-coordinate hypersurface S just outside the activated complex region is obtained by multiplication by $P_{N^+}dS$ (the relative probability of passing through an area element of S, dS in the given state N^+), by the velocity component q^r at that dS, and by the transmission coefficient $\kappa(E,N^+)$, and finally by integration over all of S and by summation over all N^+ for which the total energy does not exceed E:

$$F = \sum_{N^+} \langle \dot{q}^r \rangle \, dp_r^r \, \kappa(E,N^+)/h\Pi \qquad (2)$$

where

$$\langle \dot{q}^r \rangle = \int \dot{q}^r P_{N^+} dS.$$

The right hand side of equation (2) has to be multiplied by the summation operator γ to include all geometric and optical isomeric paths from reactants to activated complex. Upon equating equation (1) and this modified (2), noting that dE equals pdp/μ and also equals $\langle \dot{q}^r \rangle dp_r$, and finally setting p equal to $k\hbar$, equation (3) is obtained:

$$\sum_N (k^2/\pi) \, \sigma_{Np} = \gamma \sum_{N^+} \kappa(E,N^+) \qquad (3)$$

For the case when the transmission coefficient $\kappa(E,N^{+}) = 1$, for example, in classical q^{r} motion, one obtains,

$$\sum_{N}(k^{3}/\Pi)\ \sigma_{Np} = \gamma\ \sum_{N^{+}} 1. \qquad (4)$$

APPENDIX D

COMPUTATION OF THE CHARACTERISTICS OF REACTION OF BORANE WITH BORANE USING THE INDO METHOD

The characteristics of the exothermic dimerisation reaction of borane were studied by computing the minimum energy path for the approach of two borane molecules to each other with the ultimate objective of forming diborane. The computation was made using the INDO molecular orbital method which has been demonstrated[55] to be reasonably good in predicting equilibrium geometry, particularly the bond angles of molecules. So this method was justified for use in the present computation. In the computation two borane molecules were allowed to approach each other by decreasing the B-B distance, and the minimum energy configurations were found for each B-B distance. The maximum energy point along the minimum energy path corresponds to the activated complex structure for the reaction. This maximum energy minus the energy of the two reactants should give an idea of the activation energy for the reaction, however, the accuracy of this value is questionable. The essentials of the above mentioned computed data for the dimerisation reaction of borane are presented in the following Tables.

Let us define, d = distance between two boron atoms, and θ = angle of BH_a and BH_b away from the plane of the paper in opposite directions.

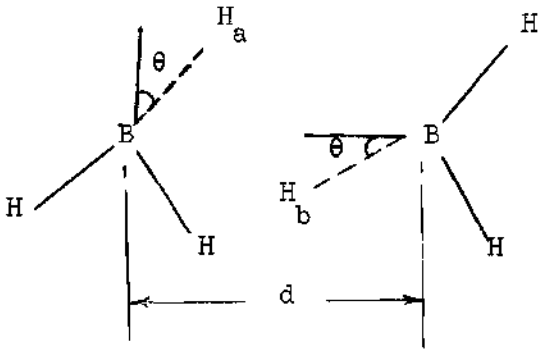

The total energy values (in Atomic Unit) have computation accuracy up to eight decimal places.

Molecular Configuration	Bond Lengths and Angles	Total Energy, A.U.	Remarks
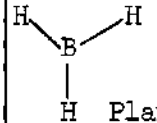 Planar	B-H length = 1.19 Å /HBH = 120°	-5.8725182658	
Two separated BH_3 molecules	ditto	-11.7450365316	
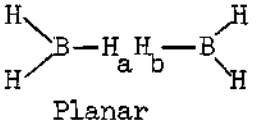 Planar	B-H length = 1.19 Å /HBH = 120° d = 4.57 Å	-11.7441223955	
ditto	ditto d = 4.27 Å	-11.7430131342	
ditto	ditto d = 4.07 Å	-11.7410172299	
ditto	ditto θ = 10° d = 4.57 Å	-11.742070881	
ditto	ditto θ = 10° d = 4.27 Å	-11.7412643697	
ditto	ditto θ = 10° d = 4.07 Å	-11.7398150517	

Molecular Configuration	Bond Lengths and Angles	Total Energy, A.U.	Remarks
ditto	ditto $\theta = 10°$ $d = 3.77$ Å	-11.7338272114	Energy increases with decrease in d and increase in θ.
ditto	ditto B-H_a length = 1.21 Å B-H_b length = 1.21 Å $\theta = 9.5°$	-11.7140622791	

The above results reveal that this may not be the minimum energy path. Similar computations were made for some other ways of approach and finally the following way of approach was found to be the minimum energy path.

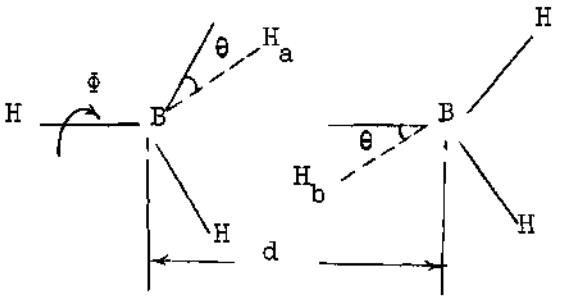

where Φ is the angle of clockwise turn of the left hand side BH_3 from the position shown above. The following Table gives the detail of computation of this minimum energy path by varying Φ, θ, and d.

Bond Lengths and Angles	Total Energy, A.U.	Total Energy Difference of the Molecule from two Separated BH_3 Molecules, kcal/mole	Remarks
B-H length = 1.19 Å /HBH = 120° d ≥ 3.40 Å Φ = 0 θ = 0	-11.7450365316	0	
ditto d = 3.35 Å	-11.7448414383	0.122	
ditto d = 3.30 Å	-11.7442675973	0.482	Energy increases with decreasing B-B distance.
ditto d = 3.20 Å	-11.7425276331	1.573	
B-H length = 1.19 Å /HBH = 120° d = 3.40 Å Φ = 10° θ = 0	-11.7432184700	1.14	
ditto θ = 5°	-11.7432760675	1.104	
ditto θ = 10°	-11.743275345	1.122	
ditto θ = 15°	-11.7426738580	1.481	
ditto θ = 2.5°	-11.7432309279	1.32	
ditto θ = 5° d = 3.35 Å	-11.7426679723	1.485	
ditto d = 3.30 Å θ = 5	-11.7418903095	1.973	
ditto d = 3.25 Å θ = 5	-11.7409073211	2.589	For Φ = 10° the minimum energy is at θ = 5°

Bond Lengths and Angles	Total Energy, A.U.	Total Energy Difference of the Molecule from two Separated BH_3 Molecules, kcal/mole	Remarks
ditto $\theta = 5°$ $d = 3.20$ Å	-11.7396773613	3.36	and d_e = 3.40 Å and the energy is -11.74-32760675 A.U.
B-H length = 1.19 Å /HBH = 120° $\Phi = 5°$ $d = 3.40$ Å $\theta = 0$	-11.7447568180	0.175	
ditto $\theta = 2.5°$	-11.7447339341	0.19	
ditto $\theta = 5°$	-11.7446621724	0.235	For $\Phi = 5°$, minimum energy is at $\theta \approx 0°$ and d_e = 3.40 Å, and the energy is -11.74475-68180 A.U.
ditto $\theta = 10°$	-11.7443816667	0.41	
B-H length = 1.19 Å /HBH = 120° $\Phi = 15°$ $d = 3.40$ Å $\theta = 0°$	11.7407118960	2.711	Energy increases with decreasing B-B distance.
ditto $d = 3.20$ Å	-11.7341743147	6.81	
ditto $d = 3.40$ Å $\theta = 5°$	-11.7409882627	2.538	
ditto $\theta = 10°$	-11.7414463793	2.251	For Φ = 15° and d_e=3.40 Å, θ=15° gives minimum energy compared to other θ values
ditto $\theta = 15°$	-11.7416092697	2.149	

Bond Lengths and Angles	Total Energy, A.U.	Total Energy Difference of the Molecule from two Separated BH_3 Molecules, kcal/mole	Remarks
ditto $\theta = 20°$	-11.7407727360	2.673	
ditto $\theta = 20°$ BH_b length = 1.22 Å	-11.7402045225	3.03	
ditto $\theta = 20°$ $B\text{-}H_a$ length =1.22 Å $B\text{-}H_b$ length =1.22 Å	-11.7393911252	3.54	So the stretching of $B\text{-}H_a$ and $B\text{-}H_b$ lengths increase the energy.
ditto $\theta = 20°$ $B\text{-}H_b$ length =1.25 Å	-11.7380465105	4.383	
ditto $\theta = 20°$ $B\text{-}H_a$ length =1.25 Å $B\text{-}H_b$ length =1.25 Å	-11.7348018620	6.417	
ditto $\theta = 10°$ $B\text{-}H_b$ length =1.22 Å	-11.7403850664	2.916	Stretching of $B\text{-}H_a$ and $B\text{-}H_b$ lengths do not minimize the energy rather increase the energy
ditto $\theta = 10°$ $B\text{-}H_a$ length =1.22 Å	-11.7393296299	3.578	
ditto $\theta = 10°$ $B\text{-}H_b$ length =1.25Å	-11.7377164432	4.59	
ditto $\theta = 10°$ $B\text{-}H_a$ length =1.25 Å $B\text{-}H_b$ length =1.25 Å	-11.7339809500	6.932	For Φ=15° and d = 3.40Å the minimum energy is

Bond Lengths and Angles	Total Energy, A.U.	Total Energy Difference of the Molecule from two Separated BH_3 Molecules, kcal/mole	Remarks
ditto θ = 10° B-H_b length=130 Å	-11.7242227071	13.05	obtained at θ=15° and the energy is -11.7416-092697 A.U. The next step is to decrease the B-B distance.
B-H length = 1.19 Å /HBH = 120° Φ = 15° θ = 15° d = 3.35 Å	-11.7417450691	2.064	Energy decreases with decrease in B-B distance.
ditto θ = 15° d = 3.30 Å	-11.7418630565	1.99	
ditto d = 3.25 Å	-11.7419588429	1.93	
ditto d = 3.20 Å	-11.7420288766	1.886	
ditto d = 3.15 Å	-11.7420713944	1.859	For Φ=15° and θ=15° minimum energy is obtained at a B-B distance of d=3.10 Å, a further decrease in d increases the energy. The minimum energy
ditto d = 3.10 Å	-11.7420877534	1.849	
ditto d = 3.05 Å	-11.7420843691	1.851	
ditto d = 3.00 Å	-11.7420753723	1.857	
/HBH = 120° B-H length =1.19 Å Φ = 20° d = 3.40 Å θ = 0°	-11.7370686928	4.996	

Bond Lengths and Angles	Total Energy, A.U.	Total Energy Difference of the Molecule from two Separated BH_3 Molecules, kcal/mole	Remarks
			is -11.74-20877534 A.U.
ditto θ= 10°	-11.7384757792	4.113	For Φ=20° and d= 3.40Å minimum energy is obtained at θ=20°. The next step is to decrease B-B distance at θ=20°.
ditto θ = 15°	-11.7398858886	3.229	
ditto θ = 20°	-11.7399578547	3.184	
ditto θ = 25°	-11.7383365450	4.201	
ditto θ = 20° d = 3.30 Å	-11.741525674	2.201	
ditto θ = 20° d = 3.20 Å	-11.7435607442	0.925	For θ=20° and Φ=20° the minimum energy is lower than that of the two reactants.
ditto θ = 20° d = 3.10 Å	-11.7462714941	-0.774	
ditto θ = 20° d = 3.00 Å	-11.7500021273	-3.113	
ditto θ = 20° d = 2.90 Å	-11.7553131397	-6.443	
B-H length = 1.19 Å /HBH = 120° $\bar{\Phi}$ = 30° d = 3.40 Å θ = 0°	-11.7262243789	11.795	
ditto d = 3.20 Å θ = 0°	-11.705899084l	2.454	

Bond Lengths and Angles	Total Energy, A.U.	Total Energy Difference of the Molecule from two Separated BH_3 Molecules, kcal/mole	Remarks
ditto d = 3.40 Å θ = 20°	-11.7373054723	4.847	
ditto d = 3.40 Å θ = 25°	-11.7376045337	4.659	For Φ=30° and d=3.40Å θ=25° gives minimum energy. Stretching of $B-H_a$ and $B-H_b$ lengths increase the energy. The next step is to decrease d at θ=25°.
ditto θ = 30°	-11.7352333827	6.146	
ditto θ = 15°	-11.7347989122	6.419	
ditto θ = 20° $B-H_a$ length and $B-H_b$ length each equal to 1.22 Å	-11.7355841375	5.927	
ditto θ = 20° $B-H_a$ and $B-H_b$ length = 1.25 Å	-11.7306583970	9.015	
ditto θ = 25° d = 3.30 Å	-11.7407423584	2.692	Energy decreases with decrease in d.
ditto θ = 25° d = 3.20 Å	-11.7449986120	0.024	
ditto θ = 25° d = 3.10 Å	-11.7508362199	-3.636	For Φ=30° and θ=25° the minimum energy is lower than the energy of the two reactants.
ditto θ = 25° d = 3.00 Å	-11.7589205817	-8.705	

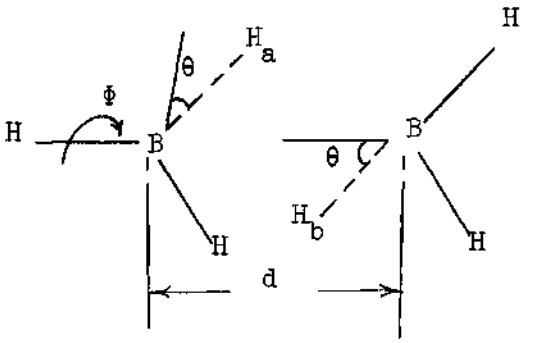

So the minimum energy path is the approach of two BH_3 molecules as shown in the figure up to a B-B distance of 3.40 Å, and then simultaneous change in the angle Φ for the left hand side BH_3 molecule, change in the angle θ for both the BH_3 molecules, and decrease in B-B distance.

The maximum energy point on the minimum energy path has the configuration as follows:

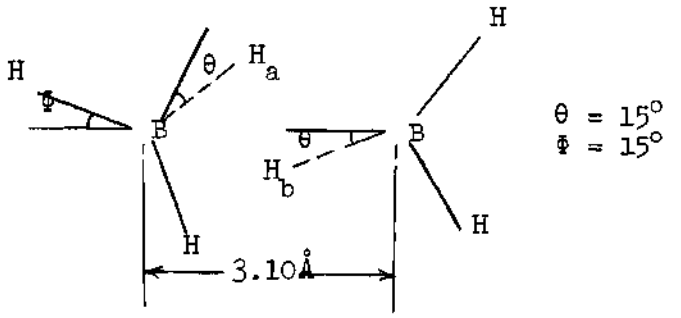

This structure can be described as the activated complex structure for the reaction. This activated complex has a total energy which is 1.849 kcal higher than that of the two BH_3 molecules. So according to this calculation, the activation energy for the reaction is 1.849 kcal/mole.

APPENDIX E

APPROXIMATE REACTION CROSS-SECTION AT THRESHOLD REGION

The general integral equation[59] applicable at the threshold region is given by,

$$\int_{E_n=0}^{E} \left[\frac{\omega(E_n)}{(2j_1+1)(2j_2+1)} \sum_{j=|j_1-j_2|}^{j_{min}} (2j+1)\, S\,(E - E_n - E_j^+) \right] dE_n =$$

$$\int_{\epsilon_{N^+}=0}^{E} \omega^+(\epsilon_{N^+})d\epsilon_{N^+} \text{ (at fixed v)}$$

where $S(E - E_n - E_j^+)$ is the contribution of the path to $(k^2/\pi)\sigma_{vnp}$. Here j_1 and j_2 are the rotational angular momentum quantum numbers for the two reactants. The meaning of the notations used here have been described in chapter II of part II.

Since the vibrational modes of the reactants are assumed to be adiabatic, n denotes (j, m_j) so that $E_n = E_j$ and $\omega(E_n)$ equals A_{rot}. So the above equation reduces to

$$\int_{E_j=0}^{E} \left[\frac{A_{rot}}{(2j_1+1)(2j_2+1)} \sum_{j=|j_1-j_2|}^{j_1+j_2} (2j+1)\, S\,(E - E_j - E_j^+) \right] dE_j =$$

$$\int_{\epsilon_{N^+}=0}^{E} \omega^+(\epsilon_{N^+})d\epsilon_{N^+}$$

Introduce a change of variable from E_j to $x(= E - E_j - E_j^+)$. Consider the activated complex as a diatomic molecule with the two reactant molecules as two atoms at the two ends of a bond. Let us denote the moment of inertia of this diatomic structure by I^+ which considers only the large moments of inertia of the complex. Let I denote the sum of the moment of inertias of the two reactant molecules around the principal axes considered in case of the activated complex. Based on these approximations, we get, for $x = E - E_j - E_j^+$, $dx = - dE_j(I^+ + I)/I^+$.

$$\frac{A_{rot}\, I^+}{I^+ + I} \int_{E_j = 0}^{E} \left[\frac{1}{(2j_1 + 1)(2j_2 + 1)} \sum_{j = |j_1 - j_2|}^{j_1 + j_2} (2j + 1)\, S\,(E - E_j - E_j^+) \right] dE_j = \int_{\epsilon_{N^+} = 0}^{E} \omega^+(\epsilon_{N^+}) d\epsilon_{N^+}$$

where it was valid to replace the lower limit of $x = I\,E/I^+$ by $x = 0$ since S is zero in the interval $(-I\,E/I^+, 0)$. Differentiation of both sides of the above equation with respect to E yields an expression for $S(u)$ for any u. Upon evaluating it at $u = E - E_j - E_j^+$, we get,

$$\frac{A_{rot}\, I^+}{(I + I^+)(2j_1 + 1)(2j_2 + 1)} \sum_{j = |j_1 - j_2|}^{j_1 + j_2} (2j + 1)\, S\,(E - E_j - E_j^+) = \omega^+(E - E_j - E_j^+).$$

Using equation (2) of Chapter I for this case, i.e., $(k^2/\pi)\sigma_{vjp} = \gamma\, S(E - E_j - E_j^+)$ to the above equation and rearranging, we obtain,

$$\frac{1}{(2j_1 + 1)(2j_2 + 1)} \sum_{j = |j_1\ j_2|}^{j_1 + j_2} (2j + 1)\, \sigma_{vjp} = \left(\frac{\pi}{k^2}\right) \frac{\gamma(I + I^+)}{A_{rot} I^+}\ \omega^+(E - E_j - E_j^+).$$

Since these equations are valid only when both E and E_j are small, one should consider only the small values of j_1 and j_2 and neglect the higher values. Let us assume that for the small values of j_1 and j_2, $S(E - E_j - E_j^+)$ and so σ_{vjp} have some average constant values with respect to j_1 and j_2. So the above expression for σ_{vjp} reduces to

$$\sigma_{vjp} = \frac{\gamma(\pi/k^2)}{C_1}[(I + I^+)/(A_{rot} I^+)]\ \omega^+(E - E_j - E_j^+)$$

where C_1 is a factor depending upon j_1 and j_2. Upon neglect of rotation-vibration interaction and dependence of q_r^+ on N^+, we get, for our case,

$$\omega(E - E_j - E_j^+) = A_{rot}^+/h\nu'.$$

Using this relation in the above expression for σ_{vjp}, we get,

$$\sigma_{vjp} = \frac{\gamma(\pi/k^2)}{C_1}\ \{(I + I^+)/A_{rot} h\nu'\}\left(\frac{A_{rot}^+}{I^+}\right)$$

When $I^+ \gg I$, the reaction cross-sections at threshold and outside threshold regions are about the same.

BIBLIOGRAPHY*

1. J. H. Wilson, Ph.D. Thesis, Georgia Institute of Technology (1966).

2. G. E. Leroi, Ph.D. Thesis, Harvard University (1960).

3. A. B. Baylis, G. A. Pressley, Jr., M. E. Gordon, and F. E. Stafford, J. Am. Chem. Soc. 88, 929 (1966).

4. T. P. Fehler and W. S. Koski, J. Am. Chem. Soc. 86, 2733 (1964).

5. A. B. Baylis, G. A. Pressley, Jr., and F. E. Stafford, J. Am. Chem. Soc. 88, 2428 (1966).

6. E. J. Sinke, G. A. Pressley, Jr., A. B. Baylis, and F. E. Stafford, J. Chem. Phys. 41, 2207 (1964).

7. T. P. Fehlner and W. S. Koski, J. Am. Chem. Soc. 87, 409 (1965).

8. T. P. Fehlner and G. W. Mappes, J. Phys. Chem. 73, 873 (1969).

9. O. Herstad, G. A. Pressley, Jr., and F. E. Stafford, A. C. S. Great Lakes Regional Meeting, June 5, 1969.

10. L. Z. Bolz, F. A. Mauer, and H. S. Peiser, J. Chem. Phys. 31, 1005 (1959).

11. J. H. Wilson and H. A. McGee, Jr., J. Chem. Phys. 46, 1444 (1967).

12. H. A. McGee, Jr., T. J. Malone, and W. J. Martin, Rev. Sci. Instr. 37, 561 (1966).

13. S. H. Bauer, J. Am. Chem. Soc. 78, 5775 (1956).

14. R. E. McCoy and S. H. Bauer, J. Am. Chem. Soc. 78, 2061 (1956).

15. A. B. Burg, J. Am. Chem. Soc. 74, 3482 (1952).

16. M. E. Garabedian and S. W. Benson, J. Am. Chem. Soc. 86, 176 (1964).

*Abbreviations follow the form described in Chemical Abstracts, Supplement (1967).

17. A. B. Burg and Y. C. Fu, J. Am. Chem. Soc. 88, 1147, (1966).

18. S. H. Garnett, Ph.D. Thesis, Princeton University (1968).

19. R. T. Holzmann, Ed., "Production of the Boranes and Related Research," Academic Press, Inc., New York, N. Y., 1967.

20. R. E. Hollins and F. E. Stafford, Inorganic Chemistry 9, 877 (1970).

21. W. J. Martin, Ph.D. Thesis, Georgia Institute of Technology (1965).

22. T. J. Malone, Ph.D. Thesis, Georgia Institute of Technology (1966).

23. J. K. Holzhauer and H. A. McGee, Jr., Anal. Chem. 41, 24A (1969).

24. A. B. Burg, J. Am. Chem. Soc. 59, 780 (1937).

25. H. D. Smyth, Proc. Roy. Soc. (London) A102, 283 (1922).

26. J. W. Warren, Nature 165, 810 (1950).

27. R. E. Honig. J. Chem. Phys. 16, 105 (1948).

28. F. P. Lossing, A. W. Tickner, and W. A. Bryce, J. Chem. Phys. 19, 1254 (1951).

29. S. N. Foner and R. L. Hudson, J. Chem. Phys. 25, 602 (1956).

30. V. H. Dibeler and R. M. Reese, J. Res. Natl. Bur. Std. 54, 127 (1955).

31. P. T. Smith, Phys. Rev. 36, 1293 (1930).

32. E. M. Clarke, Can. J. Phys. 32, 764 (1954).

33. R. E. Fox, W. M. Hickam, T. Kjeldaas, and D. J. Grove, Phys. Rev. 34, 859 (1951).

34. J. D. Morrison, (a) J. Chem. Phys. 21, 1767 (1953); (b) ibid 22, 1219 (1954).

35. R. J. Holt, Ph.D. Thesis, Georgia Institute of Technology (1969).

36. R. F. Pattie, A. J. Lorquet, and W. H. Hamill, J. Am. Chem. Soc. 84, 529 (1962).

37. J. L. Franklin, P. M. Hierl, and D. A. Whan, J. Chem. Phys. 47 (9), 3148 (1967).

38. M. A. Haney and J. L. Franklin, J. Chem. Phys. 48 (9), 4093 (1968).

39. F. E. Stafford, G. A. Pressley, Jr., and A. B. Baylis, Advan. Chem. Ser. 72, 137 (1966).

40. N. C. Baird and M. J. S. Dewar, J. Chem. Phys. 50, 1262 (1969); N. C. Baird, M. J. S. Dewar, and R. Sustman, ibid. 50, 1275 (1969); and in a continuing series of papers.

41. V. H. Dibeler, J. A. Walker, and K. E. McCulloh, J. Chem. Phys. 51, 4230 (1969).

42. G. M. Almy and R. B. Horstall, Phys. Rev. 51, 491 (1937).

43. A. C. Hurley, Proc. Roy. Soc. (London) A261, 237 (1961).

44. A Theoretical value obtained by F. P. Boer, M. D. Newton, and W. N. Lipscomb, J. Am. Chem. Soc. 88, 2361 (1966). The same bond distance was obtained from an INDO calculation on an assumed plane BH_3 molecule.

45. A. H. Nielson, J. Chem. Phys. 22, 659 (1954).

46. V. H. Dibeler and S. K. Liston, Inorg. Chem. 7, 1742 (1968).

47. The efficacy of MINDO in calculations of ionization potentials is discussed by M. J. S. Dewar and S. D. Worley, J. Chem. Phys. 50, 654 (1969).

48. R. F. Porter and S. K. Wason, J. Phys. Chem. 69, 2208 (1965).

49. R. Onaka, J. Chem. Phys. 27, 374 (1957).

50. C. Edmiston and K. Ruedenberg, J. Chem. Phys. 43, S97 (1965).

51. D. L. Hilderbrand and E. Murad, J. Chem. Phys. 43, 1400 (1965).

52. J. Blauer, M. A. Greenbaum, and M. Farber, J. Phys. Chem. 68, 2332 (1964).

53. S. Wise, J. Margrave, H. Feder, and W. Hubbard, J. Phys. Chem. 65, 2157 (1961).

54. S. H. Bauer, G. Herzberg, and J. W. C. Johns, J. Mol. Spectry. 13, 256 (1964).

55. J. A. Pople, D. L. Beveridge, and P. A. Dobosh, J. Chem. Phys. 47, 2026 (1967).

56. M. J. S. Dewar and E. Haselbach, J. Am. Chem. Soc. 92, 590 (1970).

57. J. A. Pople, D. P. Santry, and G. A. Segal, J. Chem. Phys. 43, S129 (1956); J. A. Pople and G. A. Segal, ibid 43, S 136 (1965); J. A. Pople and G. A. Segal, ibid 44, 3289 (1966); D. P. Santry and G. A. Segal, ibid 47, 158 (1967).

58. R. A. Marcus, J. Chem. Phys. 45, 2138 (1966).

59. R. A. Marcus, J. Chem. Phys. 45, 2630 (1966); R. A. Marcus, ibid 46, 959 (1967).

60. T. S. Ree, T. Ree, H. Eyring, and T. Fueno, J. Chem. Phys. 36, 281 (1962).

61. M. A. Eliason and J. O. Hirschfelder, J. Chem. Phys. 30, 1426 (1959).

62. S. W. Benson, "The Foundations of Chemical Kinetics," McGraw-Hill, New York, 1960.

63. P. B. Ascough, J. Chem. Phys. 24, 944 (1956).

64. C. C. J. Roothaan, Rev. Mod. Phys. 23, 69 (1951).

65. J. C. Slater, Quantum Theory of Atomic Structure (McGraw-Hill Book Co., New York, 1960), Vol. I., pp. 339-342.

66. A. R. Dickerson and W. N. Lipscomb, J. Chem. Phys. 27, 212 (1957).

67. J. A. Dupont and R. Schaeffer, J. Inorg. Nucl. Chem. 15, 310 (1960).

68. R. A. Marcus, J. Chem. Phys. 20, 359 (1952).

69. O. K. Rice, "Statistical Mechanics Thermodynamics and Kinetics," (Ed. L. Pauling), W. H. Freeman and Company, San Francisco and London, 1967, pp. 555-570.

70. R. P. Bell, Trans. Faraday Soc. 55, 1 (1959).

71. E. E. Witmer, "Tabulation of a Function for Calculating the Rotational Energy Levels of a Rigid Polyatomic Molecule," University of Pennsylvania Thermodynamics Research Lab., Tech. Rept., 1950.

72. E. Wigner, Z. Physik. Chem. B 19, 203 (1932).

73. H. S. Johnston, "Gas Phase Reaction Rate Theory," The Ronald Press Company, New York, 1966, p-44.

74. H. S. Johnston, Advances in Chemical Physics 3, 131 (1960).

75. W. N. Lipscomb, "Boron Hydrides," W. A. Benjamin, Inc., New York, 1963, p-275.

VITA

Partha Sarathi Ganguli was born in Durgapur, West Bengal, India on May 1, 1942. He attended Ramsagar High School and later Vishnupur High School, and graduated in 1957. He entered Ramananda College (Vishnupur) in 1957 and completed the I.Sc. course of Calcutta University in 1959. He entered Jadavpur University, Calcutta, in 1959 and was awarded the degree of Bachelor of Chemical Engineering in 1963.

In September, 1963, he enrolled in the Graduate Division of the Indian Institute of Technology (Kharagpur) and completed requirements for the Master of Technology in Chemical Engineering in August, 1965. In September, 1965, he came to the United States to enroll in the Graduate Division of the Carnegie Institute of Technology and completed requirements for the degree of Master of Science in Chemical Engineering in June, 1966. In September, 1966, he enrolled at Georgia Tech for graduate studies towards a Ph.D. degree in Chemical Engineering.

All of his graduate studies and part of his undergraduate studies were supported by the schools concerned. He has published two papers in the Journal of Chemical Physics. He plans for postdoctoral work in the near future.